J. Fluid Mech. (2001), *vol.* 428, *pp.* 213–248. Printed in the United Kingdom

One-point turbulence structure tensors

By S. C. KASSINOS[1], W. C. REYNOLDS[1,2] AND M. M. ROGERS[2]

[1]Department of Mechanical Engineering, Stanford University, Stanford, CA 94305-3030, USA
[2]NASA Ames Research Center, Moffett Field, CA 94035, USA

(Received 6 January 1999 and in revised form 3 August 2000)

The dynamics of the evolution of turbulence statistics depend on the structure of the turbulence. For example, wavenumber anisotropy in homogeneous turbulence is known to affect both the interaction between large and small scales (Kida & Hunt 1989), and the non-local effects of the pressure–strain-rate correlation in the one-point Reynolds stress equations (Reynolds 1989; Cambon *et al.* 1992). Good quantitative measures of turbulence structure are easy to construct using two-point or spectral data, but one-point measures are needed for the Reynolds-averaged modelling of engineering flows. Here we introduce a systematic framework for exploring the role of turbulence structure in the evolution of one-point turbulence statistics. Five one-point statistical measures of the energy-containing turbulence structure are introduced and used with direct numerical simulations to analyse the role of turbulence structure in several cases of homogeneous and inhomogeneous turbulence undergoing diverse modes of mean deformation. The one-point structure tensors are found to be useful descriptors of turbulence structure, and lead to a deeper understanding of some rather surprising observations from DNS and experiments.

1. Introduction

1.1. *Overview*

The goal of the one-point Reynolds-averaged theory of turbulence, initiated by Osborne Reynolds' 1895 classic paper, is the prediction of the turbulence stresses needed in the mean flow equations. Today engineering analyses of systems involving turbulent flows rely primarily on one-point Reynolds-averaged turbulence models. In simple flows, where the deformation rates are mild and the turbulence has time to reach an equilibrium with the mean flow, eddy-viscosity models have been used with success. In such flows the Reynolds stresses are determined by the applied strain rate and it is reasonable to relate them to the mean strain rate S_{ij} through the eddy-viscosity assumption,

$$R_{ij} = \frac{2k}{3}\delta_{ij} - 2\nu_\tau S_{ij}, \qquad \nu_\tau = C_\mu k^2/\varepsilon. \tag{1.1}$$

In the modern family of k–ε models, the eddy viscosity ν_τ is modelled in terms of the turbulent kinetic energy k (hereafter $q^2 = 2k$ will be used) and dissipation rate ε, for which partial differential equations (PDE) are used. Such models have proven to be very useful in predicting near-equilibrium or decaying turbulent flows, where the deformation rate $S = \sqrt{S_{ij}S_{ji}}$ is small relative to (or even comparable to) the reciprocal time scale ε/q^2 of the turbulence.

The response of turbulence to rapid mean deformation ($Sq^2/\varepsilon \gg 1$), at least initially, is described by rapid distortion theory (RDT). Under RDT the nonlinear effects resulting from turbulence–turbulence interactions are neglected in the governing equations, but even when linearized in this fashion, the one-point governing equations are, in general, not closed due to the non-locality of the pressure fluctuations. In flows with rapid mean deformations, the structure takes some time to respond and eddy-viscosity models, which predict immediate response, are inadequate. Reynolds stress transport (RST) equations have been added to the PDE system used in turbulence models in an attempt to deal with this weakness. While RST models have enjoyed some success, they are not yet widely used in industry because they have not proven reliably better than simpler models.

The reason behind this failure has to do with the proper characterization of the anisotropy of the turbulence in a one-point theory. RST and other one-point approaches use the anisotropy of the turbulent stresses to characterize the anisotropy of the field. However, the departure of R_{ij} from the isotropic form $q^2\delta_{ij}/3$ is only one aspect of the anisotropy of the turbulence. Here we hope to emphasize that the turbulence can exhibit anisotropy that is dynamically significant (even for the transport of the one-point turbulent stresses) and which is not captured in the Reynolds stresses. Other one-point statistical measures of anisotropy, in addition to the anisotropy of the turbulent stress, are then needed.

The Reynolds stresses carry information about the *componentality* of the turbulence (the relative strengths of different velocity components). Roughly speaking, each large-scale structure tends to organize spatially the fluctuating motion in its vicinity, and in so doing, to eliminate gradients of the fluctuation fields in certain directions (those in which the spatial extend of the structure is significant), and to enhance gradients in other directions (those in which the spatial extend of the structure is small). Thus associated with each eddy are local axes of dependence and independence. In undeformed isotropic turbulence the various axes of dependence and independence (due to individual eddies) are oriented randomly and this means that the fluctuation field due to the ensemble of all the eddies has gradients in all three directions. Mean deformation acting on the turbulence creates structural anisotropy because it stretches and aligns the energy-containing turbulent eddies. This in turn aligns the axes of dependence and independence due to individual eddies and creates directions in which, even in a statistical sense, gradients of energy-containing fluctuations are weak. Thus by acting on the energy-containing structure mean deformation can create axes of independence that are reflected in autocorrelations of gradients of the fluctuation fields. In regions in the flow where there is one such direction of independence, the turbulence becomes two-dimensional. Note that this says nothing about the intensity of the fluctuations in that direction. Thus the anisotropy of the *dimensionality* of the turbulence is in general distinct from the anisotropy of its componentality.

Adequate characterization of the state of the turbulence also requires information about the dimensionality of the turbulence (the relative uniformity of structure in different directions), and even of additional turbulence features in some cases. Turbulence models carrying only componentality information (e.g. standard RST models) cannot possibly satisfy conditions associated with the dimensionality of the turbulence or reflect differences in dynamic behaviour associated with structures of different dimensionality (nearly isotropic turbulence vs. turbulence with strongly organized two-dimensional structures).

This fundamental realization led us to introduce three second-rank and one third-rank one-point turbulence tensors that carry the information missing from the

Reynolds stresses. These new tensors, along with Reynolds stresses, provide a minimal tensorial base for a complete one-point theory of turbulence. Not all of these tensors are important under all conditions, which explains why traditional RST models (and even simpler approaches) have enjoyed considerable success in some cases.

Here we introduce these new tensors, demonstrate their effectiveness as descriptors of the turbulence structure, and characterize the information they carry so that turbulence modellers can devise schemes for incorporating at least some of that information into their models. In § 2 we consider anisotropic homogeneous turbulence undergoing rapid mean rotation to demonstrate the need for structure information in one-point formulations. The fundamental definitions and properties of the structure tensors are introduced and discussed in §§ 3 and 4. In §§ 5–9, we use a database from direct numerical simulations (DNS) to study the structure tensors for several cases of homogeneous and inhomogeneous turbulence undergoing diverse forms of mean deformation. The examples considered demonstrate the usefulness of the structure tensors in providing an accurate description of the turbulence. In certain cases, counterintuitive results can only be explained in terms of the combined componentality–dimensionality description, which again underscores the importance of these new tensors beyond the immediate scope of turbulence modelling. Finally, § 10 summarizes the results.

2. Insights from rapid distortion analysis of homogeneous turbulence

2.1. *Componentality vs. dimensionality*

The difference between componentality and dimensionality information is nicely exhibited by the inviscid RDT of homogeneous turbulence, for which the evolution equations for the Reynolds stresses, $R_{ij} = \overline{u_i' u_j'}$, are (see for example Kida & Hunt 1989; Reynolds & Kassinos 1995)

$$\frac{\mathrm{d}R_{ij}}{\mathrm{d}t} = -G_{ik}R_{kj} - G_{jk}R_{ki} + T_{ij}^{\mathrm{rapid}}, \tag{2.1}$$

where $G_{ij} = U_{i,j}$ is the mean velocity gradient tensor and T_{ij}^{rapid} is the *rapid* pressure–strain-rate term, which results from the familiar splitting of the pressure fluctuations into 'slow' and 'rapid' parts (see Appendix A)

$$T_{ij}^{\mathrm{rapid}} = 2G_{kn}(M_{inkj} + M_{jnki}). \tag{2.2}$$

Here $\boldsymbol{M}$ is

$$M_{ijpq} \equiv \int \frac{k_p k_q}{k^2} E_{ij}(\boldsymbol{k})\, \mathrm{d}^3\boldsymbol{k}, \tag{2.3}$$

where $E_{ij}(\boldsymbol{k}) \sim \overline{\hat{u}_i(\boldsymbol{k})\hat{u}_j^*(\boldsymbol{k})}$ is the velocity spectrum tensor, $\boldsymbol{k}$ is the wavenumber vector, hats denote Fourier coefficients and the $*$ denotes a complex conjugate.† $\boldsymbol{M}$ is a fourth-rank tensor that must be modelled in terms of the tensor variables in the one-point model (Reynolds & Kassinos 1998). The two non-zero contractions of $\boldsymbol{M}$ are

$$R_{ij} = M_{ijpp} = \int E_{ij}(\boldsymbol{k})\, \mathrm{d}^3\boldsymbol{k} \quad \text{and} \quad D_{pq} = M_{iipq} = \int \frac{k_p k_q}{k^2} E_{ii}(\boldsymbol{k})\, \mathrm{d}^3\boldsymbol{k}. \tag{2.4}$$

† In homogeneous fields, discrete Fourier expansions can be used to represent individual realizations in a box of length L; then the discrete cospectrum of two fields $\boldsymbol{f}$ and $\boldsymbol{g}$ is given by $\tilde{X}_{ij}(\boldsymbol{k}) = (L/2\pi)^3 \overline{\hat{f}_i(\boldsymbol{k})\hat{g}_j^*(\boldsymbol{k})}$, where the bar represents an ensemble average over the box. The cospectrum of two fields $X_{ij}(\boldsymbol{k})$ is the limit of the discrete cospectrum $\tilde{X}_{ij}$ as $L \to \infty$. Here we use $X_{ij}(\boldsymbol{k}) \sim \overline{\hat{f}_i(\boldsymbol{k})\hat{g}_j^*(\boldsymbol{k})}$ as a shorthand notation, but the exact definition should be kept in mind.

As noted above, $\boldsymbol{R} \equiv R_{ij}$ contains the componentality information in $\boldsymbol{M}$. $\boldsymbol{D}$ describes the distribution of energy over directions in wavenumber space, i.e. the dimensionality information in $\boldsymbol{M}$. A more general definition of $\boldsymbol{D}$ will be given shortly. The importance of dimensionality information in wavenumber space has been discussed by several authors, including Townsend (1976) and Kida & Hunt (1989).† In standard RST closures (see Launder, Reece & Rodi 1975, hereafter denoted by LRR) $\boldsymbol{M}$ is modelled as a linear function of a single tensorial argument, $\tilde{\boldsymbol{r}}$, where $\tilde{r}_{ij} = r_{ij} - \delta_{ij}/3$, $r_{ij} = R_{ij}/q^2$ and $q^2 = R_{kk}$. To $O(\tilde{\boldsymbol{r}})$, the definitions and continuity condition ($M_{ijjq} = 0$) determine the model, except for one free coefficient, which has been determined by fitting experiments. If instead $\boldsymbol{M}$ is allowed to depend on both $\tilde{\boldsymbol{r}}$ and $\tilde{\boldsymbol{d}}$, where $\tilde{d}_{ij} = d_{ij} - \delta_{ij}/3$, $d_{ij} = D_{ij}/q^2$ and $q^2 = D_{kk} = R_{kk}$, then all of the model coefficients to $O(\tilde{\boldsymbol{r}}, \tilde{\boldsymbol{d}})$ are determined by the definitions and continuity (see Appendix C). Moreover, if we then set $\tilde{\boldsymbol{d}} = 0$, the resulting model in terms of $\tilde{\boldsymbol{r}}$, including the numerical coefficient, is almost exactly the same as determined by LRR's fit to experiments, for reasons that become clear later in this paper. But when $\tilde{\boldsymbol{d}} \neq 0$, both $\tilde{\boldsymbol{d}}$ and $\tilde{\boldsymbol{r}}$ influence the evolution of $\boldsymbol{R}$; both dimensionality and componentality are important to the evolution of the energy-containing eddies (see also Reynolds 1989; Cambon, Jacquin & Lubrano 1992; Reynolds & Kassinos 1995).

2.2. *Stropholysis*

Additional insight into the important structural information involving the energy-containing eddies is provided by analysis of axisymmetric turbulence. Using the methods of Robertson (1940), Kassinos & Reynolds (1994, hereafter denoted by KR94), have shown that the general form of the spectrum for turbulence axisymmetric about the x_1-axis is given by

$$\begin{aligned} E_{ij}(\boldsymbol{k}) = {} & \frac{E}{4\pi k^2}\left(\delta_{ij} - \frac{k_i k_j}{k^2}\right) \\ & + A\left[\frac{1}{2}\left(\frac{k_1^2}{k^2} - 1\right)\delta_{ij} + \frac{1}{2}\left(\frac{k_1^2}{k^2} + 1\right)\frac{k_i k_j}{k^2} - \frac{k_1(k_i\delta_{j1} + k_j\delta_{i1})}{k^2} + \delta_{i1}\delta_{j1}\right] \\ & + R\,\frac{\epsilon_{in1}k_n(k^2\delta_{j1} - k_1k_j) + \epsilon_{jn1}k_n(k^2\delta_{i1} - k_1k_i)}{2k^3} + i\frac{H}{2\pi k^2}\epsilon_{ijn}\frac{k_n}{k^2}. \end{aligned} \tag{2.5}$$

Here $E(k, k_1, t)$ is the *energy spectrum function*, $A(k, k_1, t)$ is the *anisotropy spectrum function*, $R(k, k_1, t)$ is the *rotational spectrum function*, and $H(k, k_1, t)$ is the *helicity spectrum function*. The spectrum in (2.5) differs from the formula derived by Batchelor (1946) and Chandrasekhar (1950) in the addition of the R term, which arises from the breaking of reflectional symmetry, and it is essential for turbulence subjected to mean rotation. This is nicely demonstrated by the inviscid RDT equations for the evolution of the spectrum functions (KR94), which are

$$\frac{\mathrm{d}E}{\mathrm{d}t} = 0, \quad \frac{\mathrm{d}A}{\mathrm{d}t} = 4\Omega\frac{k_1}{k}R, \quad \frac{\mathrm{d}R}{\mathrm{d}t} = -4\Omega\frac{k_1}{k}A, \quad \frac{\mathrm{d}H}{\mathrm{d}t} = 0, \tag{2.6}$$

where $\Omega \equiv \Omega_{23} = (G_{23} - G_{32})/2$ is the mean rotation rate about the axis of symmetry x_1. These show that the spectrum function R is generated by A, and will appear even if absent initially if there is any anisotropy in the initial turbulence. The sole contributor to the energy is E. One-point statistics are obtained by integrating over the wavenumber space as shown in (2.3) and (2.4). Only E and A contribute to

† For example, D_{ij} as defined here corresponds to C_{ij} in the notation of Kida & Hunt (1989).

second-rank tensors $\boldsymbol{R}$ and $\boldsymbol{D}$. The fourth-rank tensor $\boldsymbol{M}$ receives contributions from E, A, and R, and therefore if R is non-zero $\boldsymbol{M}$ contains additional information not carried by $\boldsymbol{R}$ and $\boldsymbol{D}$. We call this information *stropholysis*† information and have shown that it is associated with a fully symmetric third-rank stropholysis tensor Q^*_{ijk}. Stropholysis plays a key role in the dynamics of all turbulence subjected to mean or frame rotation.

2.3. *Summary*

The analysis above suggests that three kinds of information are important in the evolution of the turbulent stresses in homogeneous turbulence; (i) componentality information in the turbulent stresses themselves; (ii) dimensionality information available through $\boldsymbol{D}$; and (iii) information about the breaking of reflectional symmetry by mean or frame rotation carried by the stropholysis tensor $\boldsymbol{Q}^*$. With this brief motivation based on homogeneous turbulence, we next turn to general definitions of one-point tensors that contain this and other essential information.‡

3. Definitions

3.1. *The turbulence stream function*

We introduce the turbulence stream function vector Ψ'_i, defined by

$$u'_i = \epsilon_{its}\Psi'_{s,t}, \quad \Psi'_{i,i} = 0, \quad \Psi'_{i,nn} = -\omega'_i, \tag{3.1}$$

where ω'_i denotes the turbulence vorticity vector. We require Ψ'_i to be divergence-free so that the last equality of (3.1) is valid. This choice is important for the physical meaning of the resulting structure tensors (see § 3.7). Note that Ψ'_i satisfies a Poisson equation and hence, like the fluctuating pressure, carries non-local information. Using the definition (3.1), the Reynolds stress tensor R_{ij}, its associated normalized tensor r_{ij}, and its anisotropy tensor $\tilde{r}_{ij}$ are

$$R_{ij} = \overline{u'_i u'_j} = \epsilon_{ipq}\epsilon_{jts}\overline{\Psi'_{q,p}\Psi'_{s,t}}, \quad r_{ij} = R_{ij}/R_{kk} = R_{ij}/q^2, \quad \tilde{r}_{ij} = r_{ij} - \delta_{ij}/3. \tag{3.2}$$

This shows that one-point correlations of stream function gradients, like the Reynolds stresses, are dominated by the energy-containing scales. Next, we define several correlations of stream function gradients and then show that they carry useful information.

3.2. *Dimensionality*

The structure *dimensionality* tensor D_{ij}, its associated normalized tensor d_{ij} and dimensionality anisotropy tensor $\tilde{d}_{ij}$ are defined by (see Reynolds 1989, 1991)

$$D_{ij} = \overline{\Psi'_{n,i}\Psi'_{n,j}}, \quad d_{ij} = D_{ij}/D_{kk}, \quad \tilde{d}_{ij} = d_{ij} - \delta_{ij}/3. \tag{3.3}$$

The D_{ij} tensor reveals the level of two-dimensionality of the turbulence. For example, when the turbulence is independent of x_1 then $d_{11} = 0$ because none of the stream-function components varies in that direction. When the turbulence is nearly, but not

† The name stropholysis means 'breaking by rotation' (in Greek $\sigma\tau\rho o\phi\acute{\eta}$ means turn or rotation, and $\lambda\acute{\upsilon}\sigma\iota\varsigma$ means breaking or untying).

‡ The reader will find interesting the comparison of the one-point formalism developed here with the spectral formalism of Cambon & Jacquin (1989) and Cambon, Jacquin & Lubrano (1992) based on earlier work by Craya (1958) and Herring (1974). Even though they differ in scope, the two formalisms have points of contact. For example, R^e_{ij} in Cambon *et al.* (1992) is related to the dimensionality tensor by $R^e_{ij} = -\frac{1}{2}q^2\tilde{d}_{ij}$.

completely, independent of x_1 then $d_{11} \approx 0$ because there is little stream function variation in that direction. We will see that this is the signature of wall layer streaks in turbulent boundary layers.

3.3. *Circulicity*

The structure *circulicity* tensor F_{ij}, and its associated normalized tensor f_{ij} and circulicity anisotropy tensor $\tilde{f}_{ij}$ are defined by

$$F_{ij} = \overline{\Psi'_{i,n}\Psi'_{j,n}}, \quad f_{ij} = F_{ij}/F_{kk}, \quad \tilde{f}_{ij} = f_{ij} - \delta_{ij}/3. \tag{3.4}$$

The F_{ij} tensor describes the large-scale structure of the vorticity field which is most clearly seen in the case of homogeneous turbulence. In this case, the last equality in (3.1) ensures that $\Psi'_\alpha = 0$ whenever $\omega'_\alpha = 0$; when there is no large-scale circulation about the x_1-axis the turbulence stream function component $\Psi'_1 = 0$, and hence $F_{11} = 0$. On the other hand, when most of the large-scale circulation is concentrated about the x_1-axis, $f_{11} \to 1$. Note that $F_{kk} = D_{kk}$.

3.4. *Inhomogeneity*

The inhomogeneity tensor C_{ij}, its associated normalized tensor c_{ij} and inhomogeneity anisotropy tensor $\tilde{c}_{ij}$ are defined by

$$C_{ij} = \overline{\Psi'_{i,n}\Psi'_{n,j}}, \quad c_{ij} = C_{ij}/D_{kk}, \quad \tilde{c}_{ij} = c_{ij} - c_{kk}\delta_{ij}/3. \tag{3.5}$$

Note that the normalized tensor c_{ij} is defined in terms of the trace $D_{kk} = F_{kk}$, not in terms of C_{kk}. This choice is motivated by the following considerations. First, the diagonal components of $\boldsymbol{C}$, unlike those of $\boldsymbol{R}$, $\boldsymbol{D}$ and $\boldsymbol{F}$, can be either negative or positive. This lack of positive semi-definiteness in $\boldsymbol{C}$ means C_{kk} can vanish in regions of a turbulent flow, thus producing an ill-defined c_{ij} if it were used to normalize $\boldsymbol{C}$. In addition, normalizing with $D_{kk} = F_{kk}$ results in a tensor that provides a measure of the importance of inhomogeneity relative to the other one-point tensors. Another possibility would be to normalize with R_{kk}, but this choice proves problematic in wall bounded flows where R_{kk} vanishes at the wall.

One finds that C_{ij} vanishes for homogeneous turbulence by using (3.1) to write the basic definition (3.5) in the form

$$C_{ij} = (\overline{\Psi'_i\Psi'_{k,j}})_{,k}. \tag{3.6}$$

3.5. *Invariant anisotropy measures*

The anisotropy tensors $\tilde{\boldsymbol{r}}$, $\tilde{\boldsymbol{d}}$, and $\tilde{\boldsymbol{f}}$ are trace-free, and accordingly each has only two independent anisotropy-invariants. These can be formed using the general definitions

$$I_x \equiv \tilde{x}_{ii} = 0, \quad II_x \equiv -\tfrac{1}{2}\tilde{x}_{ij}\tilde{x}_{ji}, \quad III_x \equiv \tfrac{1}{3}\tilde{x}_{ij}\tilde{x}_{jk}\tilde{x}_{ki}, \tag{3.7}$$

valid for any traceless second-rank tensor $\tilde{x}_{ij}$. One can use the independent anisotropy-invariant coordinates $(III_x, -II_x)$ to map all possible states represented by these tensors (Lumley & Newman 1977). For traceless positive semi-definite tensors (like $\boldsymbol{r}$, $\boldsymbol{d}$ and $\boldsymbol{f}$) all possible states fall inside the boundaries of a triangular region, that we call the Lumley triangle. The lack of positive semi-definiteness in $\boldsymbol{c}$ means that the map of all possible states represented by $\boldsymbol{c}$ does not lie entirely within the Lumley triangle (see § 4.2).

3.6. *Stropholysis*

From the simple example of rapidly rotated homogeneous axisymmetric turbulence in § 2.2 we know that the stropholysis tensor $\boldsymbol{Q}^*$ carries information independent of

$\boldsymbol{R}$, $\boldsymbol{D}$, $\boldsymbol{F}$, and $\boldsymbol{C}$. The general definition of the third-rank fully symmetric structure *stropholysis* tensor is given by

$$Q^*_{ijk} = \tfrac{1}{6}(Q_{ijk} + Q_{jki} + Q_{kij} + Q_{ikj} + Q_{jik} + Q_{kji}), \tag{3.8}$$

where

$$Q_{ijk} = -\overline{u'_j \Psi'_{i,k}}. \tag{3.9}$$

The bi-traces of Q_{ijk} are

$$Q_{kjk} = 0, \qquad Q_{kki} = Q_{ikk} = -(\overline{u'_k \Psi'_i})_{,k}. \tag{3.10}$$

The first of these traces vanishes due to the divergence-free nature of the fluctuating stream function (see (3.1)). From (3.10), any bi-trace of the stropholysis $\boldsymbol{Q}^*$ is given by

$$Q^*_{iik} = Q^*_{iki} = Q^*_{kki} = -\tfrac{2}{3}(\overline{u'_k \Psi'_i})_{,k}, \tag{3.11}$$

which vanishes in homogeneous turbulence.

3.7. *Information carried by the structure tensors*

When considered together, D_{ij} and F_{ij} give a fairly detailed description of the turbulence structure. For example, $d_{11} \approx 0$ and $f_{11} \approx 1$ means that the dominant large-scale structures are very nearly two-dimensional eddies aligned with the x_1-axis, with motion confined in the plane normal to the eddy axis and organized in a large-scale circulation. We call structures of this type *vortical* eddies (see figure 1*a*). On the other hand, $d_{11} \approx 0$ and $f_{11} \approx 0$ corresponds to two-dimensional structures aligned with the x_1-axis; motion is confined along the eddy axis in the form of jets and wakes as opposed to circulation around the axis. We call turbulence structures of this second type *jetal* eddies (see figure 1*b*). In general, a turbulence field includes both vortical and jetal eddies, which can be correlated or uncorrelated. We refer to structures having correlated jetal and vortical motion as *helical* eddies (see figure 1*c*). In later sections (for example see § 7) these properties of D_{ij} and F_{ij} are shown using DNS data.

The second-rank dimensionality and circulicity tensors represent *one-point* correlations that carry *non-local* information about the structure of a turbulent flow. This can be demonstrated by again considering the simple problem of homogeneous turbulence subjected to mean rotation. In this case, the rapid-pressure fluctuations p^r are given by (see KR94 and Reynolds 1976)

$$\frac{1}{\rho} p^r_{,kk} = \Omega_z \omega'_z, \tag{3.12}$$

where Ω is the mean vorticity vector. Using (3.1) and (3.12), one can show that for homogeneous turbulence with uniform density $\rho(t)$

$$\frac{1}{\rho^2}\overline{p^r_{,z} p^r_{,z}} = \Omega_m \Omega_n F_{nm}. \tag{3.13}$$

Clearly in this simple case F_{ij} carries the non-local information contained in the intensity of the rapid pressure gradient.

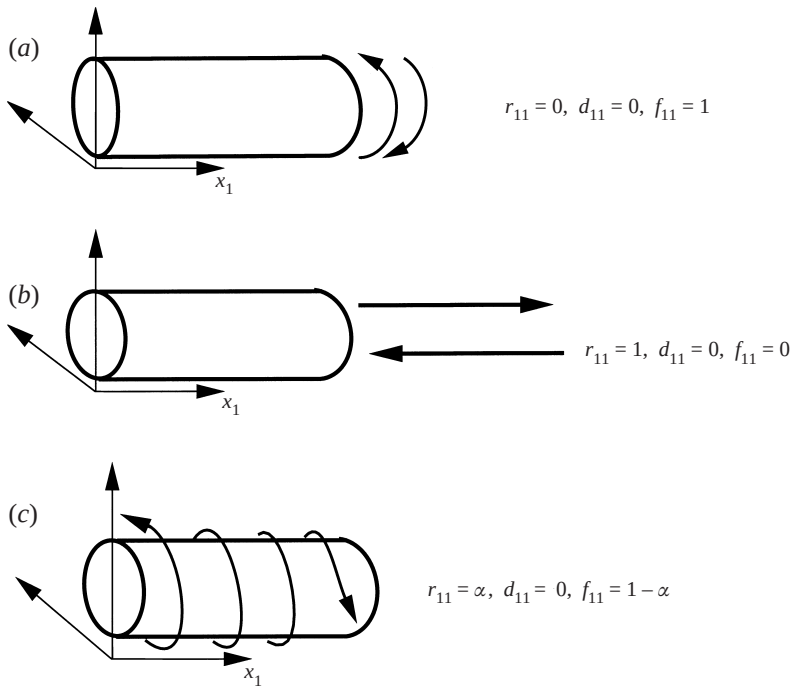

FIGURE 1. Schematic diagram showing idealized two-dimensional structures (eddies) in homogeneous turbulence and the associated componentality, dimensionality, and circulicity: (*a*) vortical eddy, (*b*) jetal eddy, and (*c*) helical eddy.

The normalized inhomogeneity tensor $\boldsymbol{c}$ reflects the degree of inhomogeneity of the turbulence field and is identically zero in homogeneous turbulence. In regions of inhomogeneous flow where inhomogeneity effects are strong one can expect at least some of the components of $\boldsymbol{c}$ to be $O(1)$, whereas in regions where local homogeneity prevails one finds that all components of $\boldsymbol{c}$ are small. Some of the examples we consider later will help clarify the role of $\boldsymbol{c}$.

In § 2.2, we saw that the third-rank stropholysis tensor Q^*_{ijk} is non-zero as a direct result of the breaking of reflectional symmetry in the velocity spectrum caused by mean rotation, hence the name *stropholysis*. The evolution equation for $\boldsymbol{Q}^*$ (see KR94 and Appendix B) and numerical simulations (see § 5) show that under *irrotational* mean strain, irrespectively of the *rate* of strain, $\boldsymbol{Q}^*$ will remain zero if it is initially zero. Only mean rotation can create $\boldsymbol{Q}^*$ and mean strain (if also present) can only act to modify $\boldsymbol{Q}^*$ once it has been generated.

Finally, note that the presence of the turbulence stream function components in these definitions means that the structure tensors cannot be easily measured in experiments. On the other hand, obtaining these tensors from direct numerical simulations is a relatively straightforward task, and this, combined with the availability of transport equations for these tensors (see KR94 and Appendix B), can lead to a better understanding of the dynamical role of the turbulence structure. This insight can in turn be used as the foundation for the formulation of simplified structure-based one-point models that incorporate the key physics without necessarily relying directly on all of these tensors and their transport equations (for example see KR94 and Reynolds & Kassinos 1995).

4. Constitutive relations and identities

The isotropic tensor identity (Jeffreys 1931; Mahoney 1985)

$$\epsilon_{ipq}\epsilon_{jts} = \delta_{ij}\delta_{pt}\delta_{qs} + \delta_{it}\delta_{ps}\delta_{qj} + \delta_{is}\delta_{pj}\delta_{qt} - \delta_{ij}\delta_{ps}\delta_{qt} - \delta_{it}\delta_{pj}\delta_{qs} - \delta_{is}\delta_{pt}\delta_{qj} \tag{4.1}$$

can be used to put (3.2) in the form

$$R_{ij} + \underbrace{\overline{\Psi'_{n,i}\Psi'_{n,j}}}_{D_{ij}} + \underbrace{\overline{\Psi'_{i,n}\Psi'_{j,n}}}_{F_{ij}} - \underbrace{(\overline{\Psi'_{i,n}\Psi'_{n,j}} + \overline{\Psi'_{j,n}\Psi'_{n,i}})}_{C_{ij}+C_{ji}} = \delta_{ij}q^2. \tag{4.2}$$

Note that (4.2) relates the turbulence stresses to the new one-point second-rank turbulence structure tensors introduced in § 3. Since three of the four tensors in (4.2) can be linearly independent, this constitutive equation offers an indication that componentality alone (found in R_{ij}) is not sufficient to completely specify the state of the turbulence. Taking the trace of (4.2) and noting that

$$F_{kk} = D_{kk}, \tag{4.3}$$

one obtains

$$C_{kk} = D_{kk} - q^2. \tag{4.4}$$

A general third-rank tensor can be decomposed into the sum of six subtensors, and the tensor $\boldsymbol{Q}$ can be represented by (see KR94)

$$Q_{ijk} = \tfrac{1}{6}q^2\epsilon_{ijk} + \tfrac{1}{3}\epsilon_{ikm}R_{mj} + \tfrac{1}{3}\epsilon_{jim}(D_{mk} - C_{mk}) + \tfrac{1}{3}\epsilon_{kjm}(F_{mi} - C_{im}) + Q^*_{ijk}. \tag{4.5}$$

Using the definitions of the second-rank tensors and (3.9), one can show that

$$R_{ij} = \epsilon_{imp}Q_{mjp}, \quad D_{ij} - C_{ij} = \epsilon_{imp}Q_{pmj}, \quad F_{ij} - C_{ji} = \epsilon_{imp}Q_{jpm}. \tag{4.6}$$

Being fully symmetric, $\boldsymbol{Q}^*$ makes no contribution to $\boldsymbol{R}$, $\boldsymbol{D}$, $\boldsymbol{F}$, and $\boldsymbol{C}$. Therefore, none of the second-rank tensors contains the information in $\boldsymbol{Q}^*$.

In the general case, the new structure tensors and the Reynolds stress tensor are related by the full forms of (4.2) and (4.5). A number of special cases exist, where additional relationships develop between these, in effect reducing the number of independent components that must be known for a full description of the state of the turbulence. Next we consider some of these special cases in detail.

4.1. *Special case: homogeneous turbulence*

For homogeneous turbulence the definition of dimensionality (3.3) has an equivalent representation in terms of the velocity spectrum tensor $E_{ij}(\boldsymbol{k}) \sim \overline{\hat{u}_i\hat{u}^*_j}$

$$D_{ij} = \int \frac{k_i k_j}{k^2} E_{nn}(\boldsymbol{k})\,\mathrm{d}^3\boldsymbol{k}, \tag{4.7}$$

where $\boldsymbol{k}$ is the wavenumber vector and $\hat{u}_i$ are the velocity Fourier components. The dimensionality D_{ij} as defined in (4.7) appears also in the work of Kida & Hunt (1989) who recognized the importance of wavenumber anisotropy in the interaction between large and small scales, and in slightly different form in the work of Cambon *et al.* (1992). Similarly, the circulicity definition (3.4) becomes

$$F_{ij} = \int \mathscr{F}_{ij}(\boldsymbol{k})\,\mathrm{d}^3\boldsymbol{k}, \quad \mathscr{F}_{ij}(\boldsymbol{k}) \sim k^2\overline{\hat{\Psi}_i\hat{\Psi}^*_j} = \frac{\overline{\hat{\omega}_i\hat{\omega}^*_j}}{k^2}, \tag{4.8}$$

where $\mathscr{F}_{ij}(\boldsymbol{k}) \sim k^2\overline{\hat{\Psi}_i\hat{\Psi}^*_j}$ is the circulicity spectrum tensor, and $\hat{\Psi}_i$ and $\hat{\omega}_i$ are the stream function and vorticity Fourier components. From (4.7), (4.8) follows that for

homogeneous turbulence

$$R_{kk} = D_{kk} = F_{kk} = q^2. \tag{4.9}$$

The inhomogeneity tensor C_{ij} vanishes in homogeneous turbulence (see (3.6)), and the fundamental constitutive equation (4.2) takes the form

$$R_{ij} + D_{ij} + F_{ij} = q^2\delta_{ij}. \tag{4.10}$$

Two tensors in (4.10) can be linearly independent. By carrying only $\boldsymbol{R}$ as a model variable, RST models effectively lump together information found in the dimensionality $\boldsymbol{D}$ and circulicity $\boldsymbol{F}$. Therefore, RST models are not always sensitive to differences in dynamic behaviour associated with the different dimensionality in homogeneous turbulence. Two one-point tensors are needed in order to capture both componentality and dimensionality information; for example one might use $\tilde{\boldsymbol{r}}$ and $\tilde{\boldsymbol{d}}$ as in the linear $\boldsymbol{M}(\tilde{\boldsymbol{r}}, \tilde{\boldsymbol{d}})$ model of Appendix C.

The analysis in § 2.2, shows that stropholysis $\boldsymbol{Q}^*$ information must also be included in the presence of mean or frame rotation, and so in Appendix C we also give a linear $\boldsymbol{M}(\tilde{\boldsymbol{r}}, \tilde{\boldsymbol{d}}, \boldsymbol{Q}^*)$ model. For homogeneous turbulence the third-rank tensor $\boldsymbol{Q}$ can be developed from the fourth-rank tensor $\boldsymbol{M}$ (see (2.3)) according to

$$Q_{ijk} = \epsilon_{ipq} M_{jqpk}. \tag{4.11}$$

Note that in this case both Q_{ijk} and Q^*_{ijk} become bi-trace free (see (3.10) and (3.11))

$$Q_{iik} = Q_{iki} = Q_{kii} = 0, \quad Q^*_{iik} = 0, \tag{4.12}$$

and because C_{ij} is zero in this case, (4.5) and (4.6) simplify into

$$Q_{ijk} = \tfrac{1}{6}q^2\epsilon_{ijk} + \tfrac{1}{3}\epsilon_{ikm}R_{mj} + \tfrac{1}{3}\epsilon_{jim}D_{mk} + \tfrac{1}{3}\epsilon_{kjm}F_{mi} + Q^*_{ijk} \tag{4.13}$$

and

$$R_{ij} = \epsilon_{imp}Q_{mjp}, \quad D_{ij} = \epsilon_{imp}Q_{pmj}, \quad F_{ij} = \epsilon_{imp}Q_{jpm}. \tag{4.14}$$

4.2. *Special case: parallel flows*

In later sections we consider DNS results from fully developed channel flow and temporally developing plane wakes and mixing layers, which are all parallel mean flows having a single direction of inhomogeneity. Here we show that in these flows theory predicts that special relationships develop between the structure tensors and the turbulence stresses. For the sake of clarity (and without the loss of generality), the direction of inhomogeneity is taken to be along the x_2-axis. Under these conditions, one can show that the inhomogeneity tensor $\boldsymbol{C}$ must be of the form

$$\boldsymbol{C} = \begin{pmatrix} C_{11} & C_{12} & C_{13} \\ 0 & C_{11} + C_{33} & 0 \\ C_{31} & C_{32} & C_{33} \end{pmatrix}. \tag{4.15}$$

Using (4.3) and (4.4) with (4.15) one can show that

$$C_{22} = \tfrac{1}{2}(D_{kk} - q^2), \tag{4.16}$$

and then using (4.16) in the (22)-component of (4.2) gives

$$R_{22} + F_{22} = D_{11} + D_{33}. \tag{4.17}$$

Realizing that $D_{kk} = F_{kk}$ in (4.16), we can also write

$$R_{22} + D_{22} = F_{11} + F_{33}. \tag{4.18}$$

In parallel flows the invariants of the anisotropy tensor $\tilde{c}_{ij}$ also satisfy special relationships. For example, it follows from (4.15) that $\tilde{c}_{ij}$ must be of the form

$$\tilde{c}_{ij} = \begin{pmatrix} \tilde{c}_{11} & \tilde{c}_{12} & \tilde{c}_{13} \\ 0 & \frac{1}{6} & 0 \\ \tilde{c}_{31} & \tilde{c}_{32} & -(\tilde{c}_{11} + \frac{1}{6}) \end{pmatrix} c_{kk}, \quad c_{kk} = C_{mm}/D_{pp}. \tag{4.19}$$

The tensor $\tilde{c}_{ij}$ in (4.19) is non-symmetric and therefore can be expressed in principal coordinates only under the condition

$$\tilde{c}_{11}(\tilde{c}_{11} + \tfrac{1}{6}) + \tilde{c}_{13}\tilde{c}_{31} + \tfrac{1}{144} \geqslant 0, \tag{4.20}$$

which guarantees three real eigenvalues for $\tilde{c}_{ij}$. Note that $\tilde{c}_{11}$, $\tilde{c}_{13}$, and $\tilde{c}_{31}$ can be positive or negative in different parts of the flow field and hence (4.20) is not a trivial condition. However, we have found (4.20) to be satisfied both in fully developed channel flow and in temporally evolving plane wakes and mixing layers. Therefore, in these flows $\tilde{\mathbf{c}}$ can be put in principal coordinates, and in these coordinates, one can show easily that the invariants of $\tilde{\mathbf{c}}$ satisfy the relationship

$$II_c\phi = 6III_c - \tfrac{1}{36}\phi^3, \qquad \phi = c_{kk}. \tag{4.21}$$

All of the key results in this section (including (4.16), (4.17) and (4.21)) have been verified using direct numerical simulations of fully developed channel flow (Kim, Moin & Moser 1987; Kim 1992, personal communication) and of temporally evolving plane wakes and mixing layers (Moser, Rogers & Ewing 1998; Rogers & Moser 1994).

4.3. *Special case: 2D–2C turbulence*

In §§ 8 and 9 we consider numerical simulations of self-similar plane wakes and mixing layers. An interesting feature of these flows is the approximate two-componentality (2C) ($r_{33} \ll r_{11}, r_{22}$) and two-dimensionality (2D) ($d_{33} \ll d_{11}, d_{22}$) that develops when external two-dimensional forcing is applied initially. In these 'forced' flows the relationships between the various structure tensors assume special forms. Here we consider an idealized 2D–2C turbulence field where the turbulent velocity components are

$$u_1' = u_1'(x_1, x_2), \qquad u_2' = u_2'(x_1, x_2). \tag{4.22}$$

In this case, the vector stream function Ψ_i' has a single non-zero component aligned with the axis of independence x_3, that is

$$\Psi_3' = \Psi_3'(x_1, x_2), \qquad \Psi_1' = \Psi_2' = 0, \tag{4.23}$$

and as result all the components of the inhomogeneity tensor C_{ij} vanish even in the presence of inhomogeneity. This feature of 2D–2C turbulence can be easily verified by writing the definition of C_{ij} in an expanded form

$$C_{ij} = \overline{\Psi_{i,k}'\Psi_{k,j}'} = \overline{\Psi_{i,1}'\Psi_{1,j}'} + \overline{\Psi_{i,2}'\Psi_{2,j}'} + \overline{\Psi_{i,3}'\Psi_{3,j}'}. \tag{4.24}$$

The first two terms on the right-hand side of (4.24) vanish because $\Psi_1' = \Psi_2' = 0$ everywhere in the field, and hence the gradients $\Psi_{1,j}'$ and $\Psi_{2,j}'$ must vanish also for all j. The last term vanishes because x_3 is an axis of independence and hence $\Psi_{i,3}' = 0$. The same facts determine the forms of the second moments, which for 2D–2C turbulence are

$$F_{ij} = \begin{pmatrix} 0 & 0 & 0 \\ 0 & 0 & 0 \\ 0 & 0 & q^2 \end{pmatrix}, \quad R_{ij} = \begin{pmatrix} q^2 - \alpha & -\beta & 0 \\ -\beta & \alpha & 0 \\ 0 & 0 & 0 \end{pmatrix}, \quad D_{ij} = \begin{pmatrix} \alpha & \beta & 0 \\ \beta & q^2 - \alpha & 0 \\ 0 & 0 & 0 \end{pmatrix}. \tag{4.25}$$

Case	Sq_0^2/ε_0	Sq^2/ε (min–max)
AXK	0.96	1.0–2.1
AXM	96.5	38.2–96.5
EXO	0.7	0.7–3.0
EXQ	70.7	47.6–70.7
PXA	1.0	1.0–3.0
PXF	154.0	63.6–154.0

TABLE 1. Parameters for the simulations of Lee & Reynolds (1985).

Here $q^2 = \overline{\Psi'_{3,1}\Psi'_{3,1}} + \overline{\Psi'_{3,2}\Psi'_{3,2}}$, $\alpha = \overline{\Psi'_{3,1}\Psi'_{3,1}}$ and $\beta = \overline{\Psi'_{3,1}\Psi'_{3,2}}$. A modified Kronecker delta tensor can be defined, such that

$$\tilde{\delta}_{ij} = \delta_{ij} - \delta_{i3}\delta_{j3} = \begin{cases} 1 & \text{if } i = j, \quad \text{for} \quad i, j = 1, 2 \\ 0 & \text{otherwise,} \end{cases} \qquad \tilde{\delta}_{ii} = 2. \tag{4.26}$$

Using (4.25),

$$D_{ij} + R_{ij} = q^2\tilde{\delta}_{ij}, \quad F_{ij} = q^2(\delta_{ij} - \tilde{\delta}_{ij}), \quad C_{ij} = 0. \tag{4.27}$$

5. Homogeneous turbulence subjected to irrotational strain

Irrotational mean deformation preserves reflectional symmetry, and as a result, the stropholysis $\boldsymbol{Q}^*$ is zero in all the flows considered in this section. RDT analysis based on the evolution equations for $\boldsymbol{R}$ and $\boldsymbol{D}$ (see KR94 and Appendix B) shows that if present initially (as for example in initially isotropic turbulence) the equality of the Reynolds stress and dimensionality anisotropies is preserved by rapid irrotational mean deformation with

$$\tilde{r}_{ij} = \tilde{d}_{ij} = -\tfrac{1}{2}\tilde{f}_{ij}. \tag{5.1}$$

Here we explore the validity of (5.1) when the irrotational mean deformation is slow.

In the discussion that follows, we use the DNS data of Lee & Reynolds (1985, hereafter denoted by LR), and consider two cases of axisymmetric contraction (AXK, AXM), two cases of axisymmetric expansion (EXO, EXQ), and two cases of plane strain (PXA, PXF). In all of these cases a constant and uniform mean strain was applied to an initially isotropic turbulence. For each flow, we have chosen the simulations corresponding to the slowest mean strain (smallest Sq_0^2/ε_0) and the most rapid mean strain (largest Sq_0^2/ε_0) as shown in table 1. Here the subscript 0 denotes initial values, and S is the mean strain rate

$$S_{ij} = \mathrm{d}\bar{U}_i/\mathrm{d}x_j, \quad S = \sqrt{S_{ij}S_{ij}/2}.$$

Following the notation of LR, we define the reference total strain by

$$C = \exp\int_0^t S\,\mathrm{d}t' = \mathrm{e}^{St}. \tag{5.2}$$

and use this as the dimensionless time variable in the discussion of evolution histories that follows.

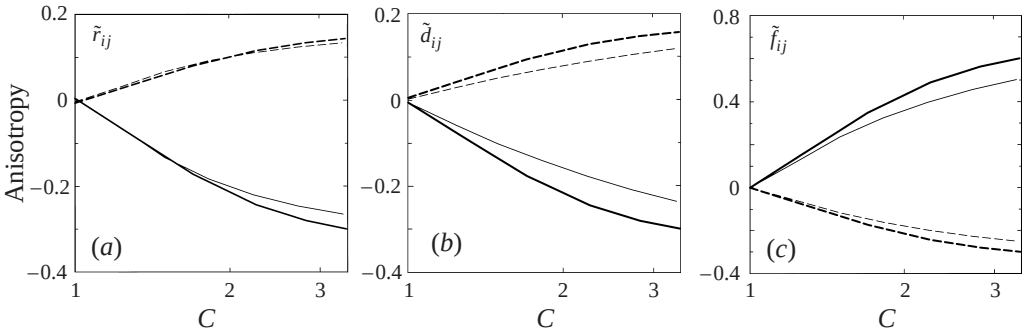

FIGURE 2. DNS results (Lee & Reynolds 1985) showing the components of (*a*) the Reynolds stress anisotropy $\tilde{r}_{ij}$, (*b*) dimensionality anisotropy $\tilde{d}_{ij}$, and (*c*) circulicity anisotropy $\tilde{f}_{ij}$ tensors in *axisymmetric contraction flow*: ——— , 11 component; – – – – , 22 and 33 components. Thin lines correspond to $Sq_0^2/\varepsilon_0 = 0.96$ (case AXK) and thick lines to $Sq_0^2/\varepsilon_0 = 96.5$ (case AXM). In this flow the eddies become aligned with the axial direction of positive mean strain x_1. The stretching of axial vorticity results in an increase of $\tilde{r}_{22}$ and $\tilde{r}_{33}$ relative to $\tilde{r}_{11}$ and an increase in the axial large-scale circulation $\tilde{f}_{11}$. In the rapidly strained case $\tilde{r}_{ij} = \tilde{d}_{ij} = -\frac{1}{2}\tilde{f}_{ij}$. The difference in the evolutions between the rapidly and slowly strained cases is relatively small. DNS data points are connected by straight lines. Case AXM agrees with RDT.

5.1. *Irrotational axisymmetric strain*

The mean strain-rate tensor considered here is of the general form

$$S_{ij} = \pm\frac{2}{\sqrt{3}}S\begin{pmatrix} 1 & 0 & 0 \\ 0 & -\frac{1}{2} & 0 \\ 0 & 0 & -\frac{1}{2} \end{pmatrix}, \quad S = \sqrt{S_{ij}S_{ij}/2}, \tag{5.3}$$

with the plus sign corresponding to the case of axisymmetric contraction and the minus sign to the case of axisymmetric expansion.

5.1.1. *Axisymmetric contraction*

The time histories of the anisotropies $\tilde{\boldsymbol{r}}$, $\tilde{\boldsymbol{d}}$, and $\tilde{\boldsymbol{f}}$ for the two cases of axisymmetric contraction are shown in figure 2. The effect of the strain on the anisotropy invariants of each tensor is shown on the anisotropy invariant maps (AIM) of figure 3, where important limiting states have been identified. The effect of the axisymmetric strain is to stretch and orient the eddies so that they tend to become aligned with the axial direction of positive strain ($S > 0$). This is accompanied by an increase in the axial large-scale circulation ($\tilde{f}_{11}$) and a decrease in the axial stress $\tilde{r}_{11}$ and dimensionality $\tilde{d}_{11}$ as the axial vorticity is being stretched. At the end of the simulations, nearly all of the large-scale circulation is concentrated around the axial direction ($f_{11} \to 1$, $\tilde{f}_{11} \to \frac{2}{3}$), and the turbulence is almost independent of the axial direction ($d_{11} \to 0$, $\tilde{d}_{11} \to -\frac{1}{3}$). Both of these effects can be explained in terms of the strong alignment of elongated vortical eddies with the axial direction. The eddy stretching and alignment are most effective in the rapid case ($Sq_0^2/\varepsilon_0 = 96.5$) where the turbulence at the end reaches an approximate 2D–2C state (see figure 3*b*). This case belongs to the RDT regime, and (5.1) holds throughout the deformation. At slower strain rates (see figure 2), the results are qualitatively similar, but note that the RDT relation (5.1) is only approximately satisfied. Yet, despite the wide difference in the initial Sq_0^2/ε_0 between the slow and rapid cases, the evolution history of the anisotropy $\tilde{\boldsymbol{f}}$ is only weakly modified when plotted against total strain. We have found that the *insensitivity of circulicity* to strain

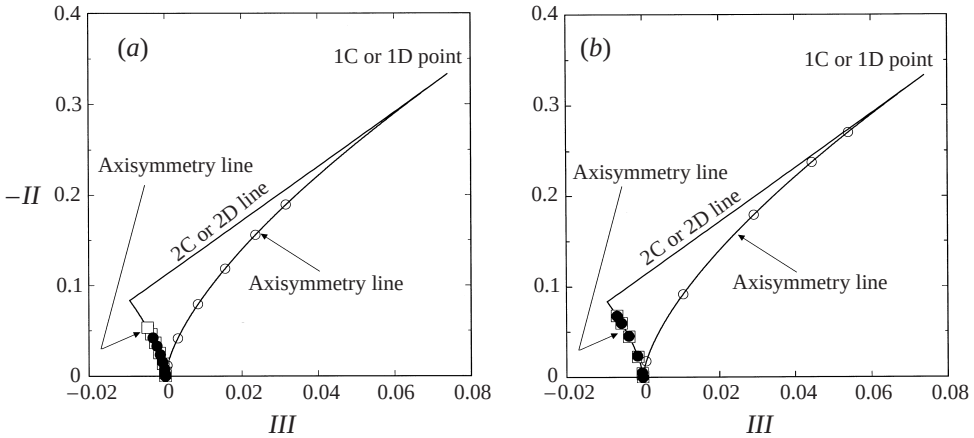

FIGURE 3. DNS results (Lee & Reynolds 1985) showing the anisotropies for the Reynolds stress (□), dimensionality (●), and circulicity tensor (○) shown on the anisotropy invariant map (AIM) for the *axisymmetric contraction flow*: (*a*) case AXK ($Sq_0^2/\varepsilon_0 = 0.96$); (*b*) case AXM ($Sq_0^2/\varepsilon_0 = 96.5$). The circulicity anisotropy follows the axisymmetry line towards the one-component point, those of the Reynolds stress and dimensionality follow the axisymmetry line towards the two-component point. In both the rapidly and slowly strained cases the circulicity anisotropy remains considerably higher than those of the Reynolds stress and dimensionality.

rate is a common feature of all the cases of irrotational mean deformation considered here. In fact, the insensitivity of circulicity has been observed in flows undergoing quite different modes of mean deformation. In figure 2 the dimensionality and Reynolds stress evolution histories are also only weakly dependent on the rate of straining, but there are cases (considered below) where these two anisotropy histories are strongly dependent on the rate of strain.

5.1.2. *Axisymmetric expansion*

The corresponding results for two cases of axisymmetric expansion are shown in figures 4 and 5. This flow exhibits counter-intuitive behaviour that makes it a challenge to turbulence modelling. The effect of the negative axial strain ($S < 0$) in these cases is to concentrate the eddies in thin, disk-like regions normal to the axis of symmetry, while the weaker positive strain causes a mild radial stretching. Sustained axisymmetric expansion produces pancake turbulence, in which the symmetry axis becomes the direction with the most energetic velocity fluctuations, but with very little large-scale circulation around it ($\tilde{f}_{11} \to -\frac{1}{3}$). As expected, in the rapid case ($Sq_0^2/\varepsilon_0 = 70.7$) the exact RDT result (5.1) holds true, and $\tilde{r}_{11} \approx \tilde{d}_{11} \to \frac{1}{6}$ towards the end of the simulation. However in the weak strain case, for which $Sq_0^2/\varepsilon_0 = 0.7$, there is a large disparity between the anisotropy of the dimensionality tensor, which is very weak ($\tilde{d}_{11} \to 0.01$), and the anisotropy of the Reynolds stress tensor, which is quite strong ($\tilde{r}_{11} \to \frac{1}{3}$). Clearly, the RDT result (5.1) is not valid in slowly strained expansion flows, which perhaps is not surprising, but note that the level of the stress anisotropy $\tilde{\boldsymbol{r}}$, shown by the square symbols on the anisotropy invariant map (AIM) in figure 5, is higher in the slower case (figure 5*a*) than it is in the rapid case (figure 5*b*). In fact the stress anisotropy reached in the slowly strained case exceeds the theoretical limit (see figure 5*b*) placed by RDT for rapid axisymmetric expansion. This result, which was noted by LR, is surprising since one would expect that the more rapid mean deformation would push the stress anisotropy to higher values. We

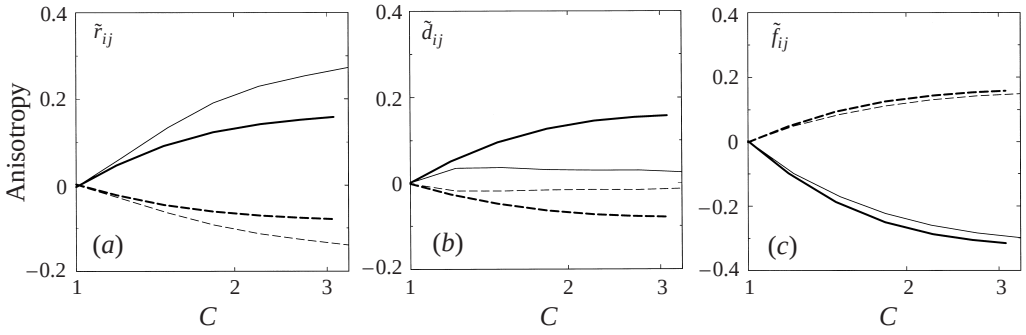

FIGURE 4. DNS results (Lee & Reynolds 1985) showing the components of (*a*) the Reynolds stress anisotropy $\tilde{r}_{ij}$, (*b*) dimensionality anisotropy $\tilde{d}_{ij}$, and (*c*) circulicity anisotropy $\tilde{f}_{ij}$ tensors in *axisymmetric expansion flow*: ——— , 11 component; – – – – , 22 and 33 components. Thin lines correspond to $Sq_0^2/\varepsilon_0 = 0.71$ (case EXO) and thick lines to $Sq_0^2/\varepsilon_0 = 70.7$ (case EXQ). In this flow the negative axial and positive lateral mean strain concentrate the eddies in thin pancake-like structures normal to the axial direction. The result is an increase of the axial Reynolds stress ($\tilde{r}_{11}$) relative to the lateral stress components, and an increase of the lateral circulicity components $\tilde{f}_{22}$ and $\tilde{f}_{33}$ relative to the axial component. In the rapidly strained case, $\tilde{r}_{ij} = \tilde{d}_{ij} = -\frac{1}{2}\tilde{f}_{ij}$. The Reynolds stresses are much more anisotropic in the slowly strained case than they are in the rapidly strained case! DNS data points are connected by straight lines. Case EXQ agrees with RDT.

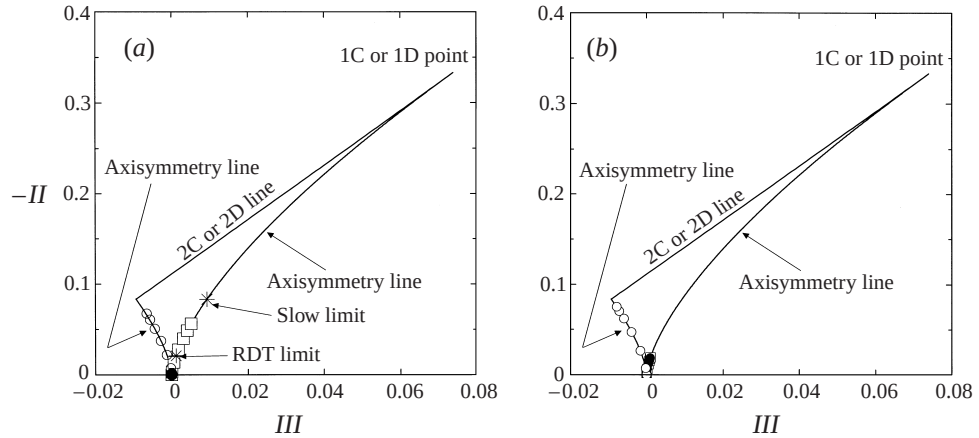

FIGURE 5. DNS results (Lee & Reynolds 1985) showing the anisotropies for the Reynolds stress (□), dimensionality (●), and circulicity tensor (○) shown on the anisotropy invariant map (AIM) for the *axisymmetric expansion flow*: (*a*) case EXO ($Sq_0^2/\varepsilon_0 = 0.71$); (*b*) case EXQ ($Sq_0^2/\varepsilon_0 = 70.7$). The anisotropies of the Reynolds stress and dimensionality fall on the axisymmetry line towards the one-component point; they are practically identical to each other in the rapidly strained case, but the anisotropy of the Reynolds stress is considerably higher that of the dimensionality in the slowly strained case. $-II_r$ reaches higher values in the slowly strained case (on the left) than it reaches in the rapidly strained case (on the right). The anisotropy of the circulicity, falling on the axisymmetry line towards the two-component line, is insensitive to the rate of straining.

see the same effect in the experimental results of Choi (1983), thus showing that this effect is not in any way related to the low Reynolds numbers of the simulations of LR. This counter-intuitive result should therefore be reflected in turbulence models. The combined stress–dimensionality–circulicity information clarifies these effects. The constitutive equation (4.10) shows that $\tilde{r}_{ij} + \tilde{d}_{ij} + \tilde{f}_{ij} = 0$; hence given the insensitivity of circulicity to strain rate (see figure 4*c*), the weak dimensionality anisotropy in

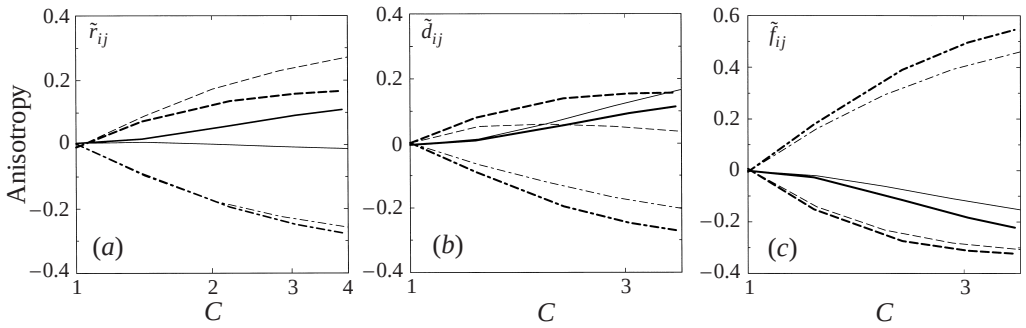

FIGURE 6. DNS results (Lee & Reynolds 1985) showing the components of the (*a*) Reynolds stress anisotropy $\tilde{r}_{ij}$, (*b*) dimensionality anisotropy $\tilde{d}_{ij}$, and (*c*) circulicity anisotropy $\tilde{f}_{ij}$ tensors in *plane strain flow*: ——— , 11 component; - - - - , 22 component; —·— , 33 component. Thin lines correspond to $Sq_0^2/\varepsilon_0 = 1.0$ (case PXA) and thick lines to $Sq_0^2/\varepsilon_0 = 154.0$ (case PXF). In this flow, the vorticity stretching in the direction of positive mean strain x_3 results in an increase in $\tilde{f}_{33}$ (large-scale circulation) and a decrease in $\tilde{r}_{33}$ and $\tilde{d}_{33}$. In the rapidly strained case, $\tilde{r}_{ij} = \tilde{d}_{ij} = -\frac{1}{2}\tilde{f}_{ij}$. Note that $\tilde{r}_{22}$ reaches higher values in the slowly strained case than it reaches in the rapidly strained case. The opposite is true for $\tilde{d}_{22}$. DNS data points are connected by straight lines. Case PXF agrees with RDT.

the slowly strained case must be compensated by an augmented stress anisotropy. Equation (4.10) can be used to place a theoretical limit to the maximum level of stress anisotropy that can be reached in the slowly strained case, corresponding to a complete vanishing of the dimensionality anisotropy ($\tilde{d}_{ij} = 0$). As shown in figure 5(*a*) the slow theoretical limit is well beyond the RDT limit.

5.2. *Plane strain*

The mean strain rate tensor for the plane strain cases has the general form

$$S_{ij} = S \begin{pmatrix} 0 & 0 & 0 \\ 0 & -1 & 0 \\ 0 & 0 & +1 \end{pmatrix}. \tag{5.4}$$

The evolution histories of the anisotropies $\tilde{\boldsymbol{r}}$, $\tilde{\boldsymbol{d}}$, and $\tilde{\boldsymbol{f}}$ are shown in figure 6 for the two different initial values of Sq^2/ε (see table 1). Sustained plane strain produces turbulence consisting of eddies elongated in the direction of positive strain ($\tilde{d}_{33} \to -\frac{1}{3}$), which have very strong circulation around their axes ($\tilde{f}_{33} \to \frac{2}{3}$), but very little motion along their axes ($\tilde{r}_{33} \to -\frac{1}{3}$). Note that this corresponds to the same 2D–2C limiting state of *vortical* eddies aligned with direction of positive strain that is produced by axisymmetric contraction. However, plane strain differs from the axisymmetric contraction flow in that the limiting state is reached along a different path in the AIM (see figure 7). As in the case of the axisymmetric expansion flows, the RDT result (5.1) is valid only in the rapid case. In all the slower cases, $\tilde{\boldsymbol{d}}$ differs significantly from $\tilde{\boldsymbol{r}}$. As in the axisymmetric strain cases, the circulicity history is insensitive to strain rate in the plane strain simulations despite the wide variation in the initial value of Sq^2/ε.

5.3. *Explanation of the slow strain effects*

Using the simulations of LR, we have shown that the RDT equality (5.1) is not valid when the mean deformation is slow. A puzzling aspect of this result is found in the axisymmetric expansion and plane strain flows, where slow strain produces a higher

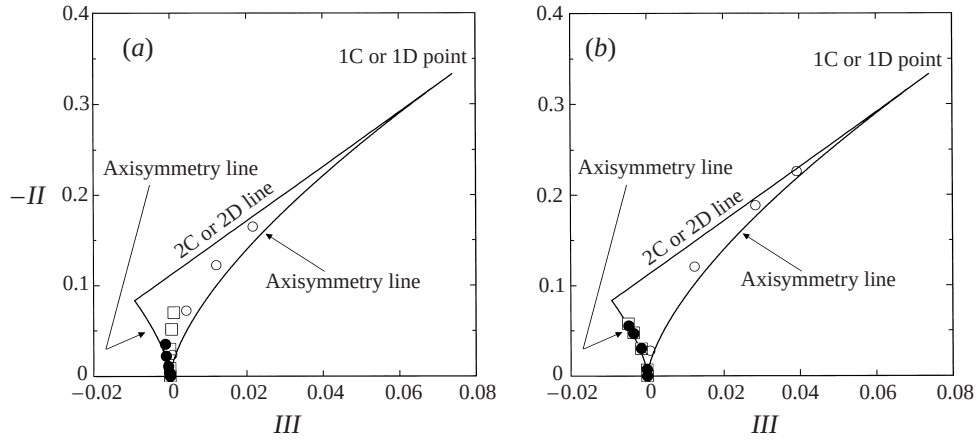

FIGURE 7. DNS results (Lee & Reynolds 1985) showing the anisotropies for the Reynolds stress (□), dimensionality (●), and circulicity tensor (○) shown on the anisotropy invariant map (AIM) for the *plane strain flow*: (*a*) case PXA ($Sq_0^2/\varepsilon_0 = 1.0$); (*b*) case PXF ($Sq_0^2/\varepsilon_0 = 154.0$). In the rapidly strained case (on the right), the anisotropies of the Reynolds stress and dimensionality are identical and fall on the axisymmetry line towards the two-component point. In the slowly strained case (on the left) the Reynolds stress anisotropy is higher than the dimensionality anisotropy and $-II_r$ reaches higher values than it reaches in the rapidly strained case (on the right). The circulicity anisotropy is relatively insensitive to the rate of straining.

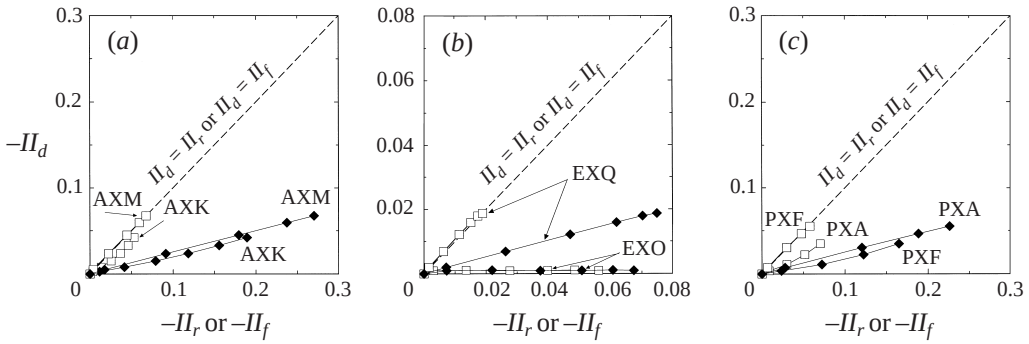

FIGURE 8. DNS results (Lee & Reynolds 1985) showing a comparison of the second invariant of $\tilde{\boldsymbol{d}}$ with the second invariants of $\tilde{\boldsymbol{r}}$ and $\tilde{\boldsymbol{f}}$ under irrotational mean deformation at different Sq^2/ϵ. (*a*) *Axisymmetric contraction*, (*b*) *axisymmetric expansion*, and (*c*) *plane strain*: □, II_d vs II_r; ◆, II_d vs II_f. The 45° dashed line represents a hypothetical case where $-II_d$ is equal to $-II_r$ or $-II_f$. The smaller the slope of a line representing actual data, the smaller the anisotropy of dimensionality ($-II_d$) is relative to the anisotropy that it is being compared to ($-II_r$ or $-II_f$). DNS data points are connected by straight lines.

level of Reynolds stress anisotropy than does rapid strain, while the opposite holds true for the dimensionality anisotropy. These effects are shown clearly in figure 8 where $-II_d$ is plotted against $-II_r$ and $-II_f$ for each of the flows (see (3.7)). These observations raise three important questions:

(i) How is it possible that $-II_r$ is bigger for slow rather than for rapid straining?

(ii) What triggers the breaking of the equality $\tilde{\boldsymbol{r}} = \tilde{\boldsymbol{d}}$ in the slow cases?

(iii) What determines which anisotropy components grow at the expense of the others?

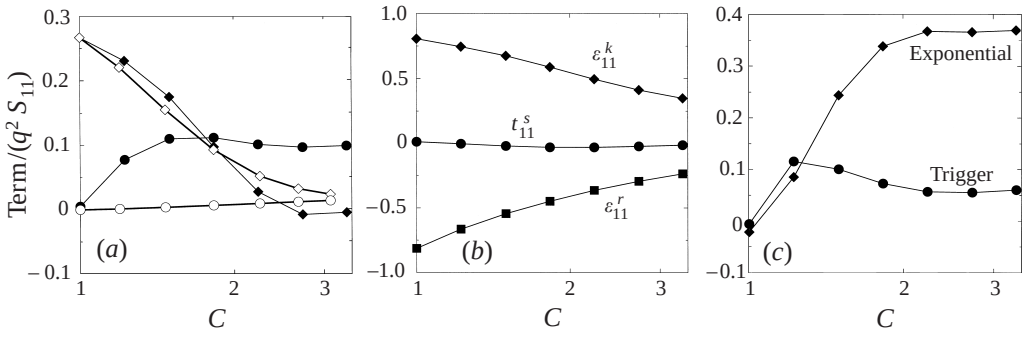

FIGURE 9. Terms contributing to the evolution of r_{11} in *axisymmetric expansion flow*. (*a*) Comparison of the total rapid (◆,◇) and slow (●,○) contributions to the evolution of r_{11} (see (5.5)); solid symbols correspond to $Sq_0^2/\varepsilon_0 = 0.71$ (case EXO), and open symbols to $Sq_0^2/\varepsilon_0 = 70.7$ (case EXQ). (*b*) Comparison of slow terms in the r_{11} equation for case EXO; (*c*) comparison of the exponential and trigger terms in equation (5.9) calculated using the DNS results of Lee & Reynolds (1985).

To answer the first question we take a closer look at the equation for r_{ij},

$$\frac{\mathrm{d}r_{ij}}{\mathrm{d}t^*} = \underbrace{p_{ij} + t^r_{ij}}_{\text{rapid}} + \underbrace{t^s_{ij} + \epsilon_{ij}}_{\text{slow}}. \tag{5.5}$$

Here $t^* = S^* t$ is the non-dimensional time based on the magnitude of the largest diagonal strain component, with $S^* = 2S/\sqrt{3}$ for axisymmetric strain, and $S^* = S$ for plane strain (see (5.3)). The rapid and slow terms on the right-hand side of (5.5) are

$$t^r_{ij} = \frac{2}{q^2 S^*} S_{nm}(M_{imnj} + M_{jmni}), \quad p_{ij} = \frac{2}{S^*} S_{nm} r_{nm} r_{ij} - \frac{1}{S^*}(S_{ik} r_{kj} + S_{jk} r_{ki}) \tag{5.6}$$

and

$$t^s_{ij} = \frac{1}{q^2 S^*} T^s_{ij}, \quad \epsilon_{ij} = \epsilon^r_{ij} + \epsilon^k_{ij}, \quad \epsilon^r_{ij} = -\frac{2\nu}{q^2 S^*}(\overline{u_{i,k} u_{j,k}}), \quad \epsilon^k_{ij} = -\epsilon^r_{mm} r_{ij}. \tag{5.7}$$

Here t^r_{ij} and t^s_{ij} are the familiar rapid and slow pressure–strain-rate terms (see (A 1)), p_{ij} is a production-rate tensor, and ϵ_{ij} a dissipation-rate tensor. For the sake of clarity, we limit our discussion to the case of axisymmetric expansion and consider only the axial component $(\,)_{11}$ of (5.5). The balance of the rapid and slow contributions in (5.5) is shown in figure 9(*a*) for both the slowly strained (EXO) and rapidly strained (EXQ) runs. Note that the contribution of the rapid terms is relatively insensitive to the rate of straining, but that of the slow terms is quite sizable in the slowly strained run and practically negligible in the rapidly strained case. Figure 9(*b*) shows the individual contributions of the various slow terms for the weak-strain run (EXO). Note that the slow pressure–strain-rate term is negligible, and hence the slow contribution is solely due to the dissipation term ϵ_{ij}. The contribution due to ϵ^r_{11} is negative as expected, but the positive contribution due to ϵ^k_{11}, which arises from the trace-normalization of the Reynolds stress tensor, is slightly larger, so that the net effect of the dissipation term is to increase r_{11}. This additional contribution due to the dissipation term in case EXO, acting to complement the rapid terms, explains how II_r can be larger in this case than in the rapid case. However, this effect does not explain why $\tilde{r}_{11}$ grows at the expense of $\tilde{d}_{11}$. The problem is that the term ϵ^k_{11}, which is the term that helps push $\tilde{r}_{11}$ to higher values, has a counterpart in the $\tilde{d}_{11}$ equation (Appendix B), which is exactly equal to ϵ^k_{11} as long as $r_{ij} = d_{ij}$. To answer the remaining questions we need

to look at the evolution equation for the anisotropy difference $\tilde{\Delta}_{ij} = \tilde{r}_{ij} - \tilde{d}_{ij}$. The transport equations for $\boldsymbol{r}$, $\boldsymbol{d}$, and $\boldsymbol{f}$ (see Appendix B) can be used to write down the evolution equation for $\tilde{\Delta}_{ij}$ for the case of homogeneous turbulence. The nonlinear terms that appear in the evolution equation for $\tilde{\Delta}_{ij}$ are found to be negligible in the simulations of LR (see Appendix B), an observation also made by Kevlahan & Hunt (1997) whose general conclusions are consistent with the present analysis. The rapid terms in the $\tilde{\Delta}_{ij}$ equation involve two fourth-rank tensors, but for a simplified analysis these may be modelled with a linear representation in $\tilde{\boldsymbol{d}}$ and $\tilde{\boldsymbol{r}}$ (see Appendix C), which is exact for weakly anisotropic turbulence. In fact for the irrotational flows considered here, this linearized representation of the rapid effects is quite accurate for $C \lesssim 3$. With these simplifying assumptions, we obtain

$$\frac{\mathrm{d}\tilde{\Delta}_{ij}}{\mathrm{d}t^*} = \frac{1}{S^*}\underbrace{\overbrace{[-\tfrac{5}{7}(S_{ik}\tilde{\Delta}_{kj} + S_{jk}\tilde{\Delta}_{ki}) + \tfrac{10}{21}S_{nm}\tilde{\Delta}_{nm}\delta_{ij} + 2S_{nm}\tilde{r}_{nm}\tilde{\Delta}_{ij}}^{\text{rapid}} - \overbrace{\epsilon^r_{mm}S^*\tilde{\Delta}_{ij}}^{\textit{slow}}]}_{\text{exponential}} + \underbrace{(\epsilon^r_{ij} - \epsilon^d_{ij})}_{\text{trigger}} \tag{5.8}$$

where $\epsilon^d_{ij} = -2\nu(\overline{u'_{k,i}u'_{k,j}})/(q^2S^*)$ and $\epsilon^d_{mm} = \epsilon^r_{mm} = -2\nu(\overline{u'_{k,i}u'_{k,i}})/(q^2S^*)$. For the case of axisymmetric expansion, the $\tilde{\Delta}_{11}$ component of (5.8) simplifies to

$$\frac{\mathrm{d}\tilde{\Delta}_{11}}{\mathrm{d}t^*} = \underbrace{[-(\tilde{r}_{11} - \tfrac{25}{21}) - \epsilon^r_{mm}S^*]\tilde{\Delta}_{11}}_{\text{exponential}} + \underbrace{(\epsilon^r_{11} - \epsilon^d_{11})}_{\text{trigger}}. \tag{5.9}$$

The terms within square brackets contribute to exponential growth. Note that the last of these terms arises from the decay of the turbulent kinetic energy and complements the effect of the rapid terms. The exponential terms, however, cannot create $\tilde{\Delta}_{ij}$ if it is initially zero. Only the last term, representing the differential dissipation of $\tilde{\boldsymbol{r}}$ and $\tilde{\boldsymbol{d}}$, can initially generate $\tilde{\Delta}_{ij}$. The *trigger* term, representing the difference between ϵ^r_{11} and ϵ^d_{11}, determines the sign of $\tilde{\Delta}_{11}$. That is to say, whether $\tilde{r}_{11}$ will grow at the expense of $\tilde{d}_{11}$ or vice versa is determined by the sign of this last term. A comparison of the exponential terms and the trigger term is shown in figure 9(*c*) for case EXO. Note that $\epsilon^r_{11} - \epsilon^d_{11} > 0$, which correctly implies that $\tilde{\Delta}_{11} = \tilde{r}_{11} - \tilde{d}_{11} > 0$. Note however, that the exponential term contributes more to the subsequent evolution of $\tilde{\Delta}_{11}$ and in the axisymmetric expansion case, an exponential growth of $\tilde{\Delta}_{11}$ is inevitable since $-(\tilde{r}_{11} - \frac{25}{21}) - \epsilon^r_{mm}S^* > 0$ at all times.

These basic principles can help explain the difference between the various $\tilde{r}_{ij}$ components and $\tilde{d}_{ij}$ in the case of slow plane strain and slow axisymmetric contraction. For example, in the slow axisymmetric contraction flow the exponential term is given by $(\tilde{r}_{11} - \frac{25}{21})\tilde{\Delta}_{11}$, and because $(\tilde{r}_{11} - \frac{25}{21}) - \epsilon^r_{mm}S^* < 0$ at all times the exponential term suppresses any $\tilde{\Delta}_{ij}$ produced by the different rates of dissipation for $\tilde{r}_{ij}$ and $\tilde{d}_{ij}$.

5.4. *Return to isotropy?*

Interesting behaviour is also encountered upon removal of the mean strain following axisymmetric expansion and plane strain. In their simulations LR found a return to isotropy of the Reynolds stresses upon removal of the mean straining following an axisymmetric contraction. However, for turbulence that had been previously distorted by an axisymmetric expansion (pancake turbulence) they found a slight increase in

the stress anisotropy following removal of the mean straining. Similarly, for the case of plane strain, they found that some of the components of the stress anisotropy increased while others decreased after the removal of the mean straining. These results are consistent with the analysis of the previous section: stress anisotropy components that under slow straining grow beyond their corresponding RDT limit are also the ones which diverge from isotropy upon removal of the straining. This suggests that essentially the same structure-related mechanism that was described in the previous section is active both during the slow mean straining mode and after its removal. In the later case, the larger scales can be expected to provide an effective strain rate on smaller scales. As explained by Kida & Hunt (1989), this large-scale strain rate is more effective in stretching structures along directions in which they had been stretched by the previous mean straining. Hence, the effects that help push the Reynolds stress anisotropy to levels that exceed the RDT limit during slow straining might remain active, at least initially, after the removal of the mean straining. Unfortunately available experimental results are inconclusive on this issue. For example, in his experiments Choi (1983) found that the rate of return to isotropy after removal of the mean deformation was much smaller following axisymmetric expansion than following axisymmetric contraction. He also found that, the higher the stress anisotropy reached during the expansion mode, the slower was the subsequent rate of return to isotropy. Clearly, carefully designed numerical simulations (or experiments) are needed to clarify these subtle features, and we are currently doing these simulations.

6. Homogeneous shear flow

In the discussion that follows, we use a time-evolving hydrodynamic field (case C128U) from the direct numerical simulations of Rogers & Moin (1987). In case C128U, a fully developed stage is reached for $10 \leqslant St \leqslant 16$ during which the turbulence Reynolds number $Re_\tau = q^4/(\epsilon\nu)$ reaches values of up to 1500 and Sq^2/ϵ (where $G_{12} = S$ is the shear rate) is about 11. Three other cases produced similar results for the one-point structure tensors and are not discussed here.

The evolution histories for the normalized second-rank tensors $\boldsymbol{r}$, $\boldsymbol{d}$, and $\boldsymbol{f}$ and the third-rank normalized stropholysis tensor $\boldsymbol{q}^* = \boldsymbol{Q}^*/\boldsymbol{R}_{nn}$ are shown in figure 10. The r_{11} component of the normalized stress tensor grows at the expense of the other two normal stresses. The dominant circulicity component is f_{22}, with f_{11} and f_{33} maintaining comparable levels throughout the evolution history. In the case of the dimensionality tensor, both d_{22} and d_{33} dominate over d_{11}.

The flow appears to be reaching equilibrium towards the end of the simulation, with approximately constant Sq^2/ϵ and $\mathscr{P}/\epsilon$ and the components of $\boldsymbol{r}$ approaching values that are very close to the experimentally observed asymptotic equilibrium values (Tavoularis & Karnik 1989). For example, the final values for the second-rank tensors, corresponding to the highest Re_τ reached in the simulation, are shown in table 2. These observations suggest that equilibrium turbulence in this flow consists mainly of elongated structures, roughly aligned along the mean flow direction ($d_{11} \approx 0.20$), and with the dominant motion along the axes of the structures ($r_{11} \approx 0.50$), i.e. jetal motion. Note that $d_{22} \approx d_{33}$, which suggests that the dimensionality is close to being axisymmetric about the x_1-axis. The near axisymmetry of $\boldsymbol{d}$ is also reflected on the AIM shown in figure 11, where the anisotropy of the dimensionality tensor falls on the axisymmetry line (towards the two-dimensional point). No such near axisymmetry is observed for $\boldsymbol{r}$ and $\boldsymbol{f}$. In fact, the near axisymmetry of $\boldsymbol{d}$ is consistent with the

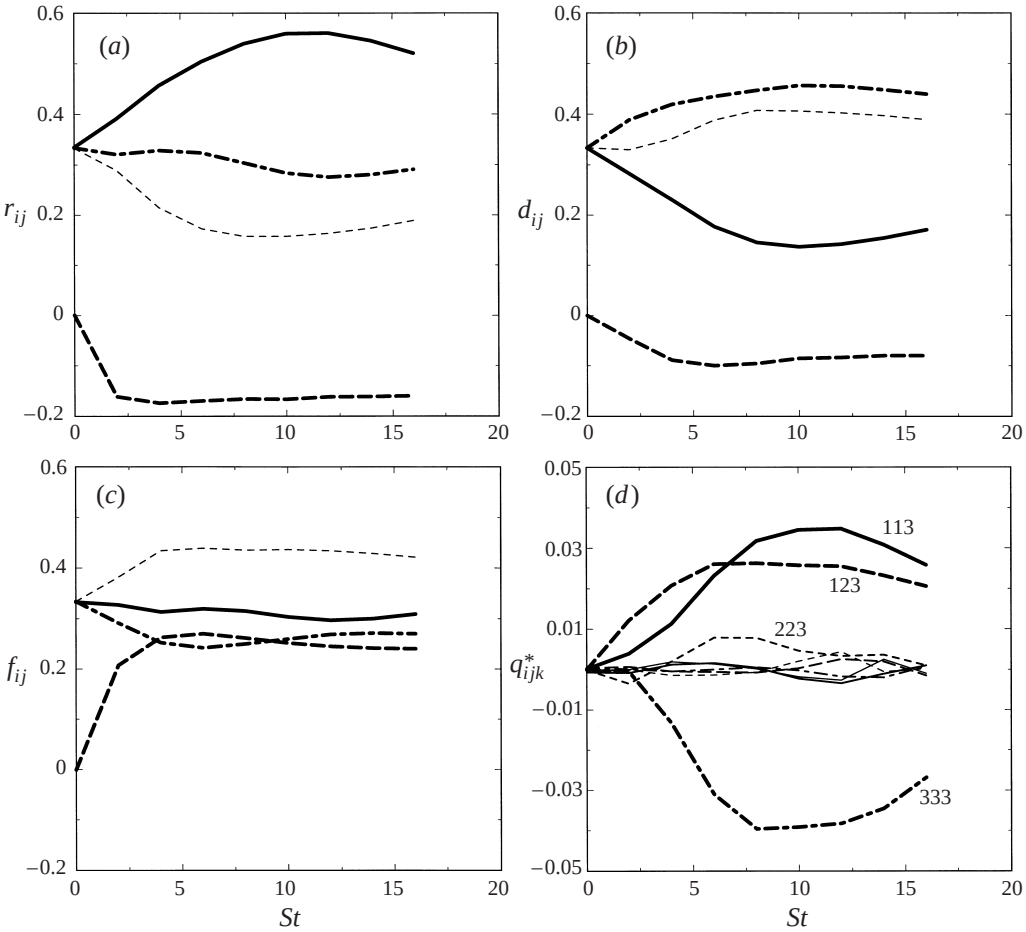

FIGURE 10. DNS results (Rogers & Moin 1987) showing the normalized Reynolds stress, circulicity, dimensionality, and stropholysis tensors for *homogeneous shear* (case C128U): ——, 11 component; - - - -, 22 component; —·—, 33 component; - - - -, 12 component. DNS data points are connected by straight lines.

ij	r^{∞}_{ij}	d^{∞}_{ij}	f^{∞}_{ij}
11	0.52	0.17	0.31
22	0.19	0.39	0.42
33	0.29	0.44	0.27
12	−0.16	−0.08	0.24

TABLE 2. Final values for $\boldsymbol{r}$, $\boldsymbol{d}$, and $\boldsymbol{f}$ from the simulations (C128U) of Rogers & Moin (1987).

hairpin-like structures with statistically axisymmetric legs observed by Rogers & Moin (1987).

A comparison of the structures in this flow to those found in the RDT limit of inviscid infinite total rapid shear is instructive. In the RDT case, the final state consists of jetal eddies (no large-scale circulation around the eddy axes) completely aligned with the streamwise direction so that $r_{11} \to 1$, $d_{11} \to 0$ and $f_{11} \to 0$. So there is a

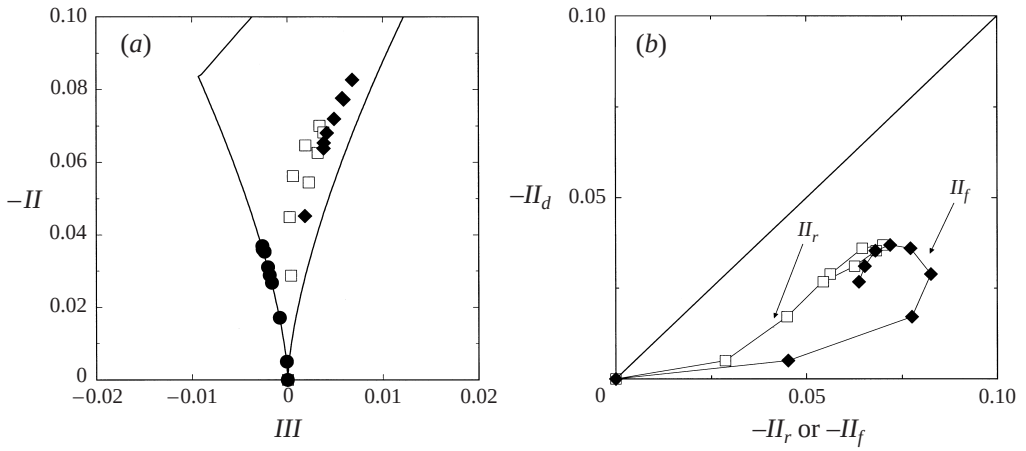

FIGURE 11. (*a*) DNS results (Rogers & Moin 1987) showing a comparison of the anisotropy of $\boldsymbol{d}$ (●) with those of $\boldsymbol{r}$ (□) and $\boldsymbol{f}$ (◆) for *homogeneous shear* (case C128U) on the anisotropy invariant map (AIM); (*b*) comparison of the second invariants of the anisotropies for case C128U. Note that the dimensionality anisotropy falls on the axisymmetry line (see *a*) and also that is considerably smaller than the Reynolds stress and circulicity anisotropies (see *a* and *b*).

marked difference in the turbulence structure in these two situations. As will be shown in § 7, the structure tensors indicate that the turbulence structure near the centreline of fully developed channel flow is similar to that found in equilibrium homogeneous shear flow.

As shown in figure 11, $\tilde{\boldsymbol{r}}$ and $\tilde{\boldsymbol{f}}$ reach anisotropy levels that are considerably higher than those reached by $\tilde{\boldsymbol{d}}$. Figure 11(*b*) shows a comparison of the second invariant $-II_d$ with $-II_r$ and $-II_f$. Clearly, the dimensionality remains more isotropic than both the Reynolds stresses and the circulicity. These results are in general agreement with what was observed in the case of irrotational strain (§ 5) where, with the exception of the RDT cases, $-II_d$ was found to be lower than both $-II_r$ and $-II_f$.

Stropholysis plays an important role in flows with strong mean rotation because it modifies the rapid pressure–strain-rate term. As shown in the plot for the normalized stropholysis tensor $q^*_{ijk} = Q^*_{ijk}/R_{nn}$ (see figure 10*d*) only q^*_{113}, q^*_{123}, and q^*_{333} (out of the nine independent components of the fully-symmetric $\boldsymbol{q}^*$ tensor) are significantly energized. These components contribute to the rapid pressure–strain-rate term (see (A 4)). Note that q^*_{113} is roughly equal to the negative of q^*_{333}, indicating a transfer of energy from r_{33} to r_{11}. One can decompose the rapid pressure–strain-rate term into three parts (see Appendix A) given by

$$T_{ij}^{\text{rapid}}/q^2 = (T_{ij}^S + T_{ij}^\omega + T_{ij}^Q)/q^2. \tag{6.1}$$

T_{ij}^S is the contribution of the mean strain, T_{ij}^w involves the explicit contribution of mean rotation, and T_{ij}^Q involves the contribution of mean rotation through stropholysis effects. Each of the three contributions T_{ij}^S, T_{ij}^ω, and T_{ij}^Q is trace-free and represents a separate intercomponent energy transfer mechanism. In figure 12 we show a comparison of the three contributions. The main role of T_{ij}^S is to drain roughly equal amounts of energy out of the R_{11} and R_{22} components and transfer it to R_{33}. The off-diagonal component T_{12}^S tends to decrease the magnitude of the shear stress R_{12}. The main role of T_{ij}^ω is simply to increase the magnitude of the shear stress R_{12}. The stropholysis part T_{ij}^Q, on the other hand, returns a third of the energy that T_{ij}^S

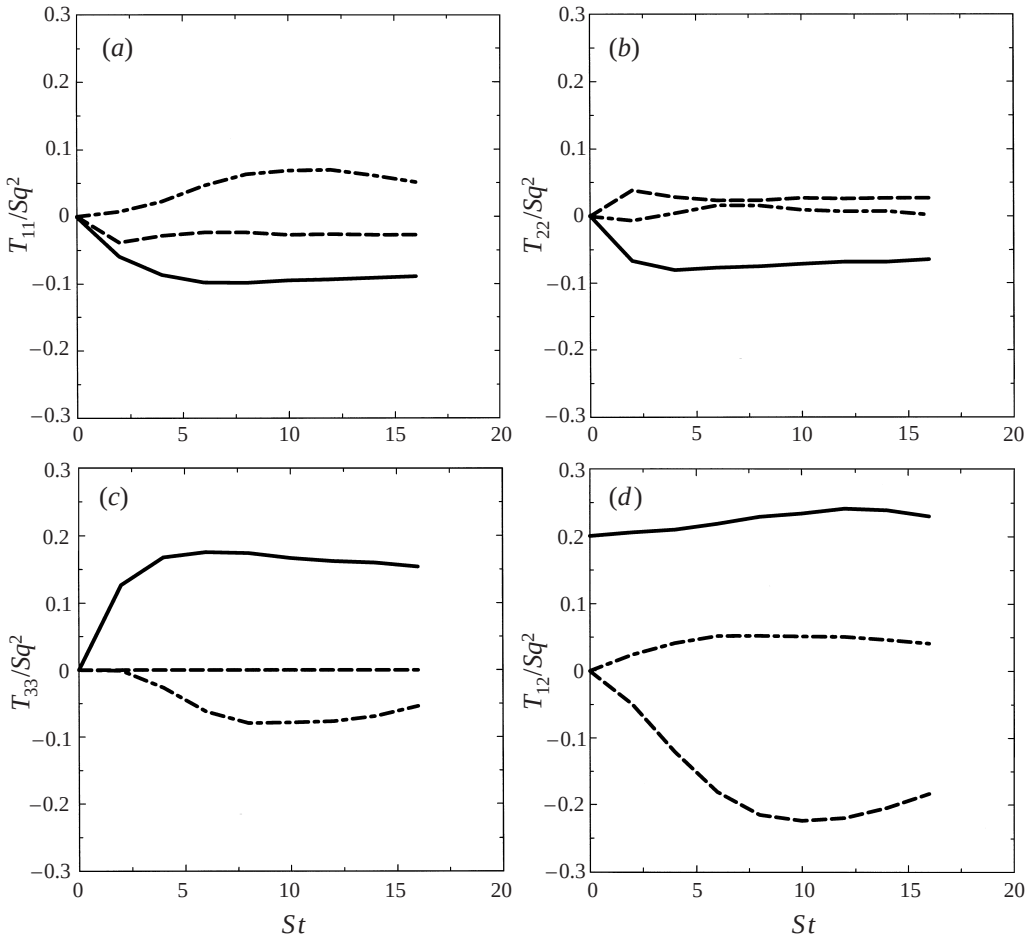

FIGURE 12. DNS results (Rogers & Moin 1987) showing the strain, explicit-rotation, and strophlysis contributions to the normalized rapid pressure–strain-rate term for *homogeneous shear* (case C128U) with $Sq_0^2/\epsilon_0 = 4.73$: ——, strain part T_{ij}^s/Sq^2; - - - -, explicit-rotation part T_{ij}^ω/Sq^2; —·—, stropholysis part T_{ij}^Q/Sq^2. T_{ij}^s/Sq^2 transfers energy out of r_{11} and r_{22} and into r_{33} (see *a*, *b*, and *c*), but T_{ij}^Q/Sq^2 returns some this energy preferentially back to r_{11}. In this case of the shear stress (see *d*), T_{ij}^s/Sq^2 and T_{ij}^Q/Sq^2 oppose the increase in shear stress magnitude that is caused by T_{ij}^ω/Sq^2. DNS data points are connected by straight lines.

transfers from R_{11} and R_{22} into R_{33} back to R_{11}. In this sense, T_{11}^S and T_{11}^Q play competing roles. The off-diagonal component T_{12}^Q acts to decrease the magnitude of R_{12}, thereby reinforcing the effect of T_{12}^S. This example underscores the challenge faced by turbulence modellers who have to devise ways to capture some stropholysis effects, even though these are not completely parametrized by second moments like $\boldsymbol{r}$ and $\boldsymbol{d}$.

7. Fully developed channel flow

We begin our study of the structure tensors in inhomogeneous flows with the direct numerical simulations of fully developed channel flow by Kim, Moin & Moser (1987), and Kim (1992). These simulations have Reynolds numbers based on the wall shear

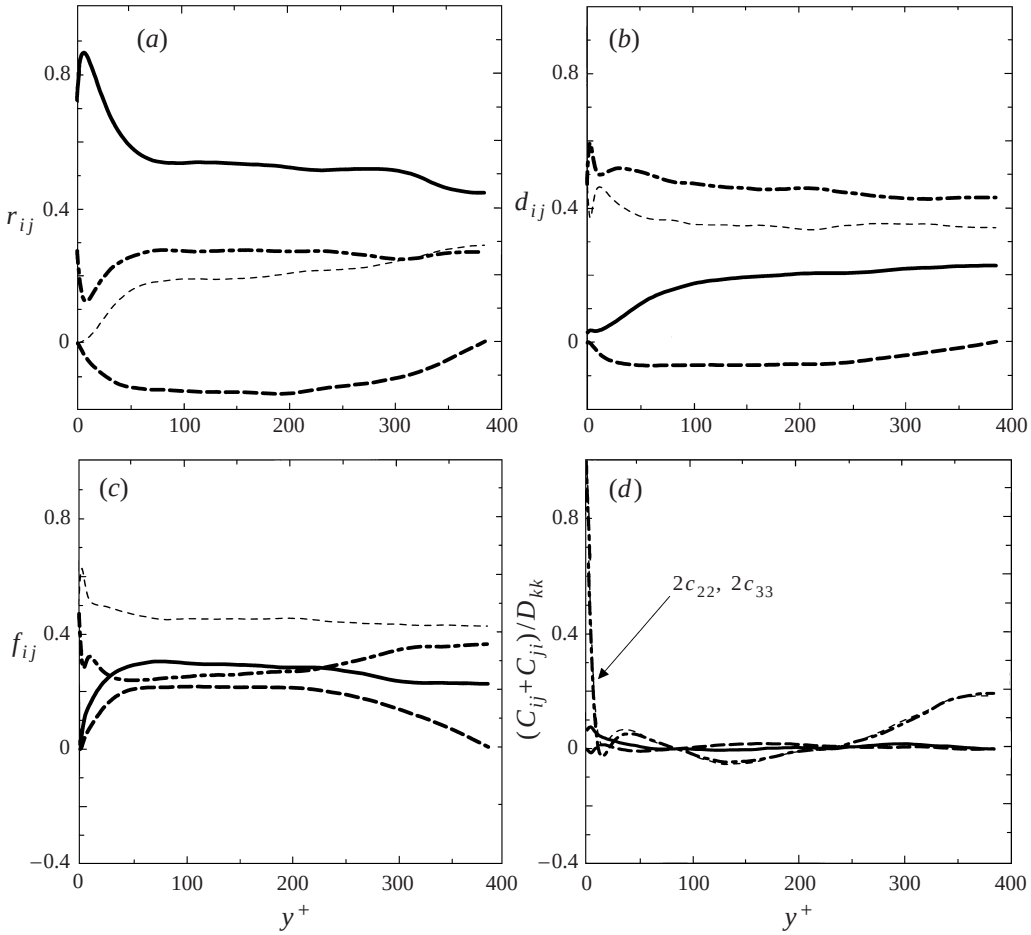

FIGURE 13. DNS results (Kim 1992) showing the normalized Reynolds stress, circulicity, dimensionality, and inhomogeneity tensors in *fully developed channel flow* with $Re_\tau = 385$: ——, 11 component; - - - -, 22 component; —·—, 33 component; - - - -, 12 component. Near the wall $d_{11} \ll r_{11}$ and $f_{11} \ll r_{11}$ reflecting the strong jetal character of the near-wall structures. For $y^+ \gtrsim 100$ the profiles look similar to those obtained in homogeneous shear flow. Inhomogeneity is confined to the near-wall region, with the log-region appearing locally homogeneous.

velocity u_τ of $Re_\tau = 180$ and $Re_\tau = 385$. In both cases, we take x_1 and x_3 to be the homogeneous streamwise and spanwise directions, and x_2 to be the wall-normal direction.

The profiles of the normalized Reynolds stress, dimensionality, circulicity, and symmetrized inhomogeneity tensors are shown in figure 13 for $Re_\tau = 385$. The corresponding results from the $Re_\tau = 180$ case were qualitatively similar and are not shown here, but some minor differences that were observed are discussed. Because the flow is statistically symmetric about the channel centreline, the statistical sample in these profiles was effectively doubled by averaging the two channel halves together. The dominant component of the Reynolds stress tensor r_{11}, corresponding to the fraction of turbulent kinetic energy found in streamwise fluctuations, reaches a maximum at $y^+ \approx 8$. The streamwise component d_{11} is smaller than r_{11} throughout the channel,

Near-wall region, $y^+ = 3.5$				Channel centreline			
ij	r_{ij}	d_{ij}	f_{ij}	ij	r_{ij}	d_{ij}	f_{ij}
11	0.84	0.03	0.09	11	0.44	0.23	0.22
22	0.00	0.38	0.62	22	0.29	0.34	0.42
33	0.16	0.59	0.29	33	0.27	0.43	0.36
12	−0.02	0.00	0.03	12	0.00	0.00	0.00

TABLE 3. Structure tensors in fully developed channel flow at $Re_\tau = 385$ (Kim *et al.* 1987).

indicating the presence of large-scale structures that are preferentially elongated in the streamwise direction.

The components of the three normalized tensors in the near-wall region (at $y^+ = 3.5$) and at the channel centreline are shown in table 3 for the $Re_\tau = 385$ case (with almost identical values found in the $Re_\tau = 180$ case). Based on these values one can argue that the near-wall structures are nearly two-dimensional ($d_{11} \approx 0$) and roughly aligned with the wall ($r_{12} \approx 0$, $d_{12} \approx 0$), have a strong jetal character ($r_{11} \gg r_{22}, r_{33}$), very little circulation around their axes ($f_{11} \ll 1$), and roughly a circular cross-section since $d_{22} \approx d_{33}$. These results are indicative of the streaky structures in the near-wall region of the channel, which have been observed directly both experimentally (for example see Smith & Metzler 1983) and in numerical simulations, including those of Kim *et al.* (1987). In contrast, near the channel centreline the normalized tensors (see table 3) give a quite different picture of the turbulence structure. The streamwise component d_{11} is lower than d_{22} and d_{33}, but only moderately so, indicating that the large-scale structures are only somewhat elongated in the streamwise direction. f_{11} is only moderately lower than f_{22} and f_{33}, suggesting that the jetal character of these structures is much less pronounced at the centreline than in the near-wall region. Note that these centreline values are not far from the equilibrium values of the three tensors in homogeneous shear flow, as estimated from the simulations of Rogers & Moin (1987) (see table 2).

The profiles of the symmetrized inhomogeneity tensor, normalized by D_{kk} to give a measure of the relative importance of inhomogeneity, are shown in figure 13(*d*). As expected, $c_{ij}+c_{ji}$ is large in the near-wall region ($y^+ \lesssim 30$), indicating a strong degree of inhomogeneity there. A similar inhomogeneity profile was obtained in the $Re_\tau = 180$ case, but in that case inhomogeneity values were somewhat more pronounced in the region $10 \lesssim y^+ \lesssim 30$. A small residual inhomogeneity also seems to exist at the channel centreline in both cases, which can be attributed to the gradual vanishing of Sq^2/ϵ (with increasing y^+) as the channel centreline is approached. Note, however, that *the flow in the log-region is locally homogeneous*, with the higher Re_τ case reaching a local homogeneity closer to the wall. Local homogeneity in the log-region has been noted in the past, for example by Rogers & Moin (1987). The inhomogeneity tensor $\boldsymbol{c}$ provides a quantitative measure of this effect. The approximate vanishing of c_{ij} means that in the log-region one-point statistics, like $\boldsymbol{R}$, $\boldsymbol{D}$ and $\boldsymbol{F}$, satisfy constitutive equations normally associated with homogeneous turbulence, for example (4.9) and (4.10). This is good news for turbulence modelling.

The AIMs for $\tilde{d}_{ij}$ and $\tilde{r}_{ij}$ are shown in figure 14. The large difference between the structure of the wall-region turbulence and that of the turbulence in the central core is reflected in the AIM for $\tilde{d}_{ij}$. The jetal character of the wall-region structure is also apparent from the AIM for $\tilde{r}_{ij}$. Consistent with the trend observed in homogeneous

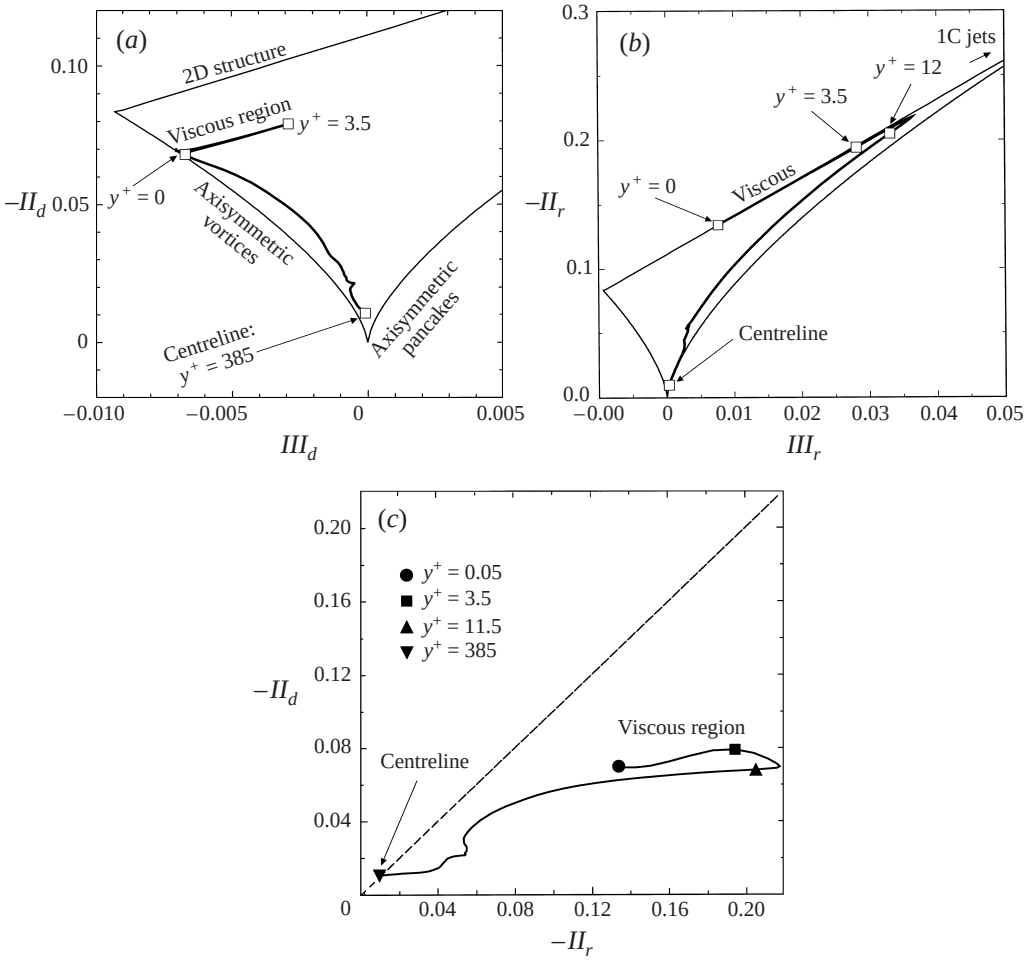

FIGURE 14. DNS results (Kim 1992) showing the anisotropy invariants in *fully developed channel flow* at $Re_\tau = 385$. (*a*) anisotropy invariant map (AIM) for $\tilde{\boldsymbol{d}}$, (*b*) anisotropy invariant map for the $\tilde{\boldsymbol{r}}$, and (*c*) comparison of $-II_d$ to $-II_r$.

flows, the anisotropy of the dimensionality tensor is smaller than that of the stress tensor (see figure 14*c*) everywhere in the flow, except at the channel centreline where the two anisotropies are equal but quite small.

8. Self-similar plane wake

We consider two simulations of time-developing turbulent wakes presented by Moser *et al.* (1998). In one of the simulations, two-dimensional disturbances were added initially to mimic two-dimensional forcing. This case will be referred to here as the *forced wake*. The *unforced wake*, where no two-dimensional disturbances were added beyond what was present in the initial conditions, was allowed to evolve long enough to attain self-similarity. In the forced case no extended period of self-similar growth was obtained, but a period of approximate self-similarity was used to generate time-averaged profiles.

Following Moser *et al.* (1998) the cross-stream direction y is normalized by the wake

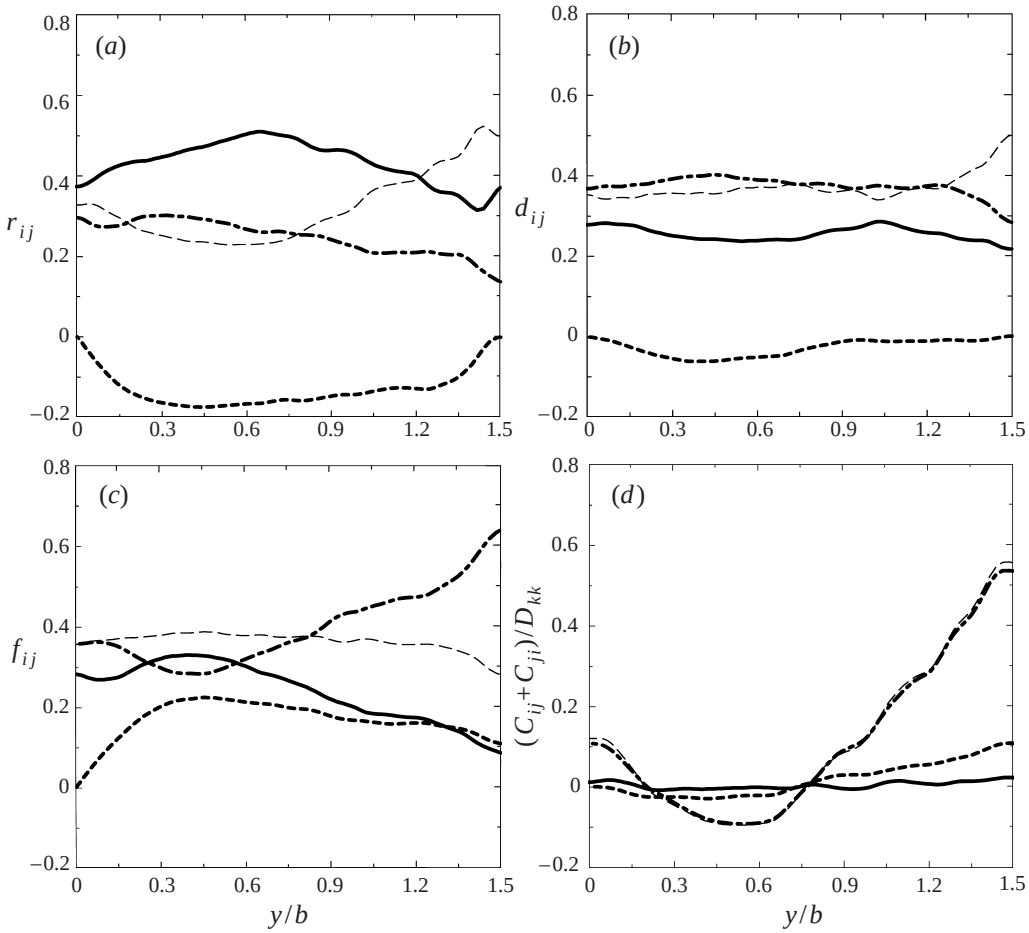

FIGURE 15. DNS results (Moser *et al.* 1998) showing the normalized Reynolds stress, circulicity, dimensionality, and inhomogeneity tensors in an *unforced plane wake* at $\tau = 91.5$ (self-similar period): ———, 11 component; - - - -, 22 component; —·—, 33 component; ----, 12 component. In the core region, the profiles are similar to those in homogeneous shear flow (see figure 10). Inhomogeneity is moderate except near the edge where it becomes significant, but there the non-normalized tensors are small.

half-width $b(t)$. The half-width is taken to be the distance between the y-locations at which the mean velocity is half of the maximum velocity deficit magnitude U_0. The non-dimensionalization of the time variable is based on the mass-flux deficit $\dot{m}$ and the initial magnitude of the velocity deficit U_d, and is given by $\tau = tU_d^2/\dot{m}$.

The normalized Reynolds stress, dimensionality, circulicity and symmetrized inhomogeneity tensors for the unforced case are shown in figure 15 for a time during the self-similar period. Since the wake is statistically symmetric, the statistical sample in these profiles was effectively doubled by averaging the two sides of the wake together. The distribution of the various tensor components is similar to what was obtained in the case of homogeneous shear flow (see figure 10). The profile for the normalized dimensionality tensor d_{ij} remains relatively constant across the wake. The streamwise component d_{11} is slightly smaller than the cross-stream and spanwise components (d_{22} and d_{33}) indicating the existence of structures that are somewhat elongated in the streamwise direction. As in the case of homogeneous shear, f_{12} attains a relatively

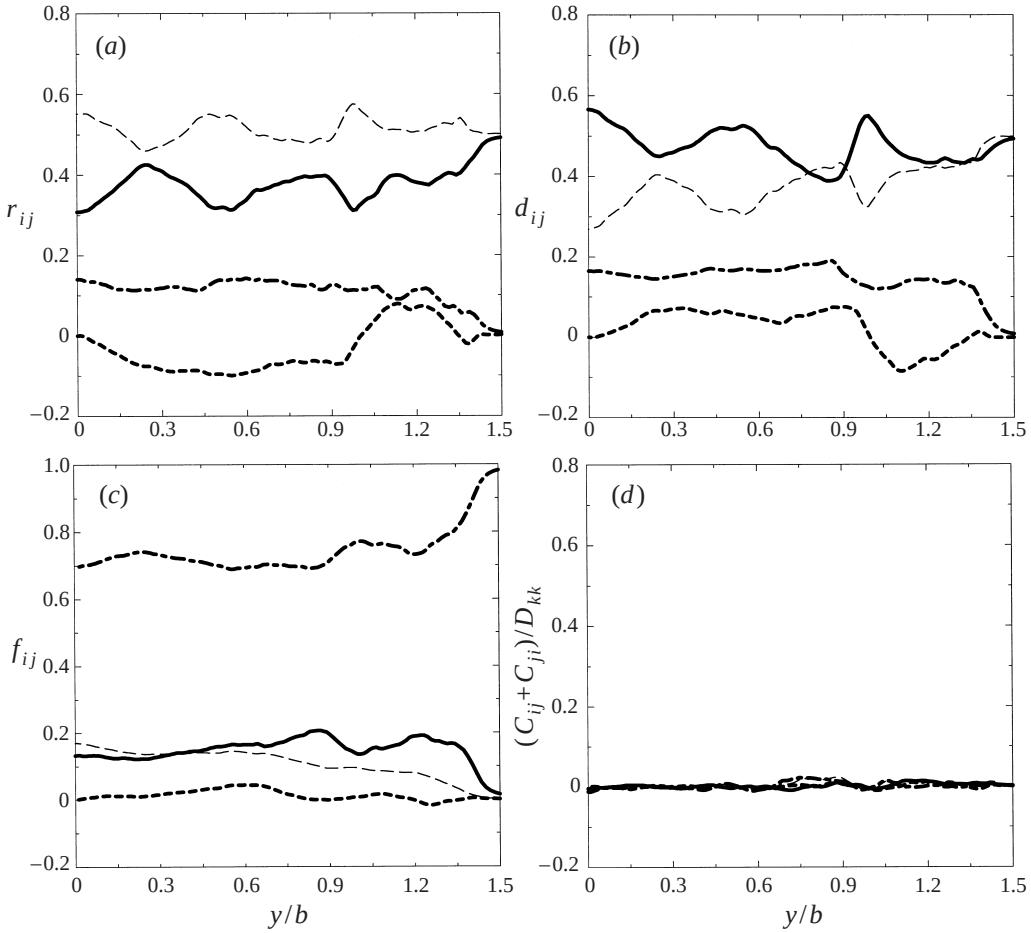

FIGURE 16. DNS results Moser *et al.* (1998) showing the normalized Reynolds stress, circulicity, dimensionality, and inhomogeneity tensors in a *forced plane wake* at $\tau = 50.0$, during the approximate self-similar period: ——— , 11 component; - - - -, 22 component; —·—, 33 component; ----, 12 component. The structure is characterized by coherent concentrations of large-scale spanwise circulation as reflected in the profiles of d_{33} and f_{33}. Two-dimensional forcing produces effectively 2D–2C turbulence, for which the inhomogeneity c_{ij} vanishes, rendering homogeneous relations among the one-point tensors valid.

constant positive value across the wake. The non-zero value of f_{12} suggests that the structures are inclined to the streamwise direction.

In figure 15(*d*) the components of the symmetrized inhomogeneity tensor are shown normalized with D_{kk} to obtain a measure of the relative significance of inhomogeneity in this flow. The profiles of $c_{ij} + c_{ji}$ suggest that the effects of inhomogeneity are moderate across most of the wake except in the potential far field where c_{22} and c_{33} grow significantly, but where all terms of the non-normalized C_{ij} (and the other tensors) are small.

The profiles of the components of the normalized tensors in the case of the forced wake are shown in figure 16, also during the (approximate) self-similar period. The striking difference between these profiles and those for the unforced wake (see figure 15) is a manifestation of the differences in the structure of the turbulence in these two flows. Moser *et al.* (1998) point out that the unforced wake is best described

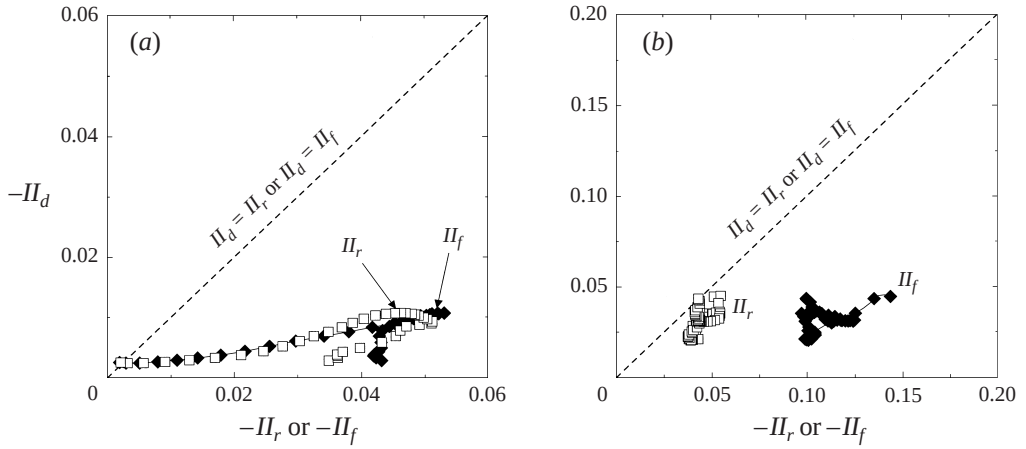

FIGURE 17. DNS results (Moser *et al.* 1998) showing a comparison of the anisotropy of $\boldsymbol{d}$ with those of $\boldsymbol{r}$ and $\boldsymbol{f}$ in (*a*) an *unforced plane wake* and (*b*) *forced plane wake*. In all cases □ corresponds to II_d vs. II_r and ◆ corresponds to II_d vs. II_f.

as 'a slab of turbulence with undulating boundaries'. In contrast, in the forced wake one can observe coherent 'concentrations of large-scale spanwise circulation'. These differences are nicely reflected in the profiles of d_{33} and f_{33} for the two cases. Note that the two-dimensional forcing has suppressed d_{33} and augmented f_{33}, as one would expect in a flow with the principal energy-containing structure consisting of vortical structures aligned with the spanwise (x_3) axis.

The most striking effect of the forcing is the emergence of relationships among the components of the four tensors that are valid across the entire wake, and which can be summarized as follows:

$$\left.\begin{aligned} &d_{11} \approx r_{22}, \quad d_{22} \approx r_{11}, \quad d_{33} \approx r_{33} \ll d_{11}, d_{22}, \quad d_{12} \approx -r_{12}, \\ &f_{33} \gg f_{11}, f_{22}, \quad f_{12} \approx 0 \quad \text{and} \quad c_{ij} + c_{ji} \approx 0 \quad \text{for} \quad i, j = 1, 2, 3. \end{aligned}\right\} \tag{8.1}$$

Note that these results are just an approximate form of the exact results discussed in §4.3 for 2D–2C turbulent flow. Hence, the forcing of the two-dimensional modes has produced a turbulent flow where the dominant energy-containing motion is very close to being 2D–2C; as a result, the effects of inhomogeneity are much less dominant in this case than in the unforced wake. Note that $c_{kk} \approx 0$, and hence $F_{kk} \approx q^2$ (see (4.3) and (4.4)), which is consistent with both the fluctuating velocity and the large-scale circulation fields being generated primarily by the same large spanwise vortical structures.

It should be emphasized that the suppression of $c_{ij} + c_{ji}$ is due to the strong 2D–2C character of this flow and does not necessarily imply vanishing of all spatial gradients of statistical moments. The suppression of the inhomogeneity tensor means that all the relationships that exist between the remaining structure tensors in homogeneous turbulence (for example (4.9) and (4.10)) are also valid locally in this case. This suggests that it should be relatively easy to extend good models for homogeneous turbulence to handle cases like this. In essence, forcing of two-dimensional modes results in a reduction in the number of independent tensor components that are required for the description of the turbulence in this flow.

Figures 17(*a*) and 17(*b*) show a comparison of $-II_d$ to $-II_r$ and $-II_f$ for the unforced and forced wakes. In the unforced wake, the anisotropies of $\boldsymbol{r}$ and $\boldsymbol{f}$ are very

close to each other and considerably higher than that of $\boldsymbol{d}$, except near the centreline of the wake, where all anisotropies are small. Note, however, that two-dimensional forcing makes the anisotropies of both $\boldsymbol{r}$ and $\boldsymbol{f}$ roughly uniform across the entire wake, and II_r approximately equals II_d, as expected for nearly 2D–2C turbulence.

9. Self-similar turbulent mixing layer

We also studied the structure tensors in self-similar turbulent mixing layers. For this purpose we used the direct numerical simulations by Rogers & Moser (1994) of two cases (forced and unforced) of a temporally evolving plane mixing layer. The conclusions reached are similar to those stated for the case of the self-similar plane wake. In the unforced plane mixing layer the profiles for all four tensors (r_{ij}, d_{ij}, f_{ij} and c_{ij}) are relatively uniform and the inhomogeneity effects are quite small except near the edges of the layer ($\xi \gtrsim 2.5$). In this inhomogeneous region, the turbulence structure in the strongly inhomogeneous region is dominated by large-scale circulation (not vorticity) about the spanwise direction. Forcing of the two-dimensional modes has the same effect on the mixing layer as in the plane wake, that is it produces a flow that is very close to being 2D–2C and that is dominated by vortical structures inducing a large-scale circulation about the spanwise direction x_3. As in the plane wake, strong forcing effectively reduces the number of independent components required to describe the turbulence.

10. Conclusion

We have introduced a systematic framework for studying the effects of turbulence structure on the evolution of one-point statistics using four one-point statistical measures of structure: the dimensionality $\boldsymbol{D}$, circulicity $\boldsymbol{F}$, inhomogeneity $\boldsymbol{C}$ and stropholysis $\boldsymbol{Q}^*$. These one-point structure tensors provide useful information about different aspects of the energy-containing turbulence structure and are useful as diagnostic tools and in turbulence modelling.

These ideas were explored using a number of numerical simulations of both homogeneous and inhomogeneous turbulence undergoing diverse modes of mean deformation. Several general trends were observed (with some variation) across all the simulations examined.

Rapid irrotational mean deformation of initially isotropic homogeneous turbulence produces identical componentality and dimensionality anisotropies ($\tilde{\boldsymbol{r}} = \tilde{\boldsymbol{d}}$). The large-scale circulation is concentrated around the axes of positive mean strain rate. This is consistent with the idea that the primary mode of deformation in rapidly strained flows is one of vortex stretching along the principal directions of positive mean strain rate.

As the rate of the irrotational mean deformation decreases, the dimensionality tends to remain closer to isotropy. However, circulicity anisotropy is relatively insensitive to the rate of mean deformation. Since the sum of the componentality, dimensionality, and circulicity anisotropies must vanish in homogeneous turbulence, one can encounter flows in which *slower* deformation produces *larger* Reynolds stress anisotropy than. This is confirmed by the DNS of LR and the experiments of Choi (1983), which show that slower mean strain rates can produce Reynolds stress anisotropies that exceed the level of anisotropy reached under RDT. The results reported by LR and Choi also provide evidence that the same stress anisotropy components which under slow straining grow beyond their corresponding RDT limit also

initially diverge further from isotropy upon removal of the strain. Carefully designed numerical simulations (or experiments) are needed to conclusively clarify these subtle features of axisymmetric expansion (and plane strain) flows.

The tendency of the anisotropy of the dimensionality to remain small under weak strain and to become significant under strong strain has important implications for turbulence modelling. It explains why turbulence models based solely on $\boldsymbol{r}$ (ignoring $\boldsymbol{d}$) work well for weakly distorted turbulence, but fail for strongly distorted turbulence. A model based on the standard return-to-isotropy assumption is insensitive to the role of structure in the return-to-isotropy problem and simply cannot be calibrated consistently for all irrotational flows.

Stropholysis plays an important role in flows with strong mean rotation by providing a separate intercomponent transfer mechanism within the rapid pressure–strain-rate term. We believe that good models for turbulence subjected to mean or frame rotation must include stropholysis information in some (perhaps simplified) form.

The inhomogeneity tensor $\boldsymbol{c}$ appears to be an effective diagnostic tool for local homogeneity in inhomogeneous turbulence. The local homogeneity in the log-region of fully developed channel flow (Rogers & Moin 1987), the weak inhomogeneity of free shear flows, as well as the strong inhomogeneity in the near-wall region are reflected in the profiles of $\boldsymbol{c}$.

The inhomogeneity tensor $\boldsymbol{c}$ vanishes in 2D–2C turbulence. The implication of this is that these flows can be treated as locally homogeneous, in the sense that all the constitutive relations among various one-point statistics that exist in homogeneous turbulence are also valid in 2D–2C turbulence.

We hope that these ideas will stimulate some innovative schemes for incorporating structure information in one-point turbulence closures. We will report our progress in this direction in due course.

The authors wish to thank Peter Bradshaw for scrutinizing the manuscript as well as the referees for suggesting a number of valuable improvements. This work has been supported by the Air Force Office of Scientific Research (Drs James McMichael, Mark Glauser and Thomas Beutner) and by the Center for Turbulence Research.

Appendix A. An exact decomposition of the rapid pressure–strain-rate term

The inviscid RDT evolution equations for the Reynolds stresses in homogeneous turbulence are given by (2.1). Closure of these equations requires modelling of the fourth-rank tensor $\boldsymbol{M}$ appearing in the rapid pressure–strain-rate term T_{ij}^{rapid} (see (2.2) and (2.3)), which results from the familiar splitting of the pressure fluctuations

$$\frac{1}{\rho}p'_{,mm} = \underbrace{-2G_{mn}u'_{n,m}}_{\text{rapid}} \quad \underbrace{-u'_{m,n}u'_{n,m} + \overline{u'_{m,n}u'_{n,m}}}_{\text{slow}}. \tag{A 1}$$

Group theory allows the decomposition of a general fourth-rank tensor into five subtensors satisfying specified symmetries and antisymmetries. This decomposition is analogous to the splitting of a second-rank tensor into its symmetric and antisymmetric parts. KR94 carried out the exact decomposition of $\boldsymbol{M}$ to isolate contributions from individual structure tensors. Based on this decomposition of $\boldsymbol{M}$, one can write the rapid pressure–strain-rate term (2.2) as

$$T_{ij}^{\text{rapid}} = T_{ij}^{S} + T_{ij}^{\Omega} \tag{A 2}$$

with

$$T_{ij}^{S} = 4S_{kn}M_{ijnk}^{*} + \tfrac{2}{3}q^{2}[S_{ij} - S_{kk}(\delta_{ij} - f_{ij}) + \delta_{ij}S_{kn}f_{nk} - (S_{ik}f_{kj} + S_{jk}f_{ki})] \tag{A 3}$$

and

$$T_{ij}^{\Omega} = T_{ij}^{w} + T_{ij}^{Q}, \quad T_{ij}^{w} = \tfrac{2}{3}q^{2}[\Omega_{im}(r_{mj} - d_{mj}) + \Omega_{jm}(r_{mi} - d_{mi})], \quad T_{ij}^{Q} = -2\Omega_{z}Q_{kij}^{*}. \tag{A 4}$$

Here $S_{ij} = (G_{ij} + G_{ji})/2$ and $\Omega_{ij} = (G_{ij} - G_{ji})/2$ are the mean strain and rotation rate tensors, and M_{ijnk}^{*} is a fully symmetric tensor that can be constructed from $\boldsymbol{M}$ according to

$$M_{ijnk}^{*} = \tfrac{1}{6}(M_{ijnk} + M_{inkj} + M_{ikjn} + M_{jkni} + M_{jnki} + M_{nkij}). \tag{A 5}$$

Equations (A 3) and (A 4) highlight the role played by the dimensionality $\boldsymbol{d}$ and the stropholysis $\boldsymbol{Q}^{*}$ in the rapid pressure–strain-rate term. In § 6, the simulations of Rogers & Moin (1987) are used to explain the role of $\boldsymbol{Q}^{*}$ in homogeneous shear flows.

Appendix B. Transport equations for the turbulence structure tensors (homogeneous turbulence)

The transport equations for the dimensionality $\boldsymbol{D}$, circulicity $\boldsymbol{F}$, and stropholysis $\boldsymbol{Q}^{*}$ can be obtained starting from the fluctuating momentum equation. Because the basic definitions for the structure tensors involve correlations between gradients of the stream function, the necessary manipulations that lead to the desired transport equations are most conveniently done in a frame of reference deforming with the mean motion, in which all the dependent turbulence statistics are homogeneous. Details of the derivation procedure can be found in KR94 and will not be repeated here. The resulting evolution equations for the dimensionality and circulicity tensors in homogeneous turbulence are

$$\frac{\bar{\mathrm{D}}D_{ij}}{\bar{\mathrm{D}}t} = -D_{ik}G_{kj} - D_{jk}G_{ki} + 2S_{mn}L_{imnj} - 2S_{mn}M_{mnij} - T_{ij}^{\mathrm{slow}} - (\overline{\Psi'_{i,m}\Psi'_{n,j}u'_{m,n}} + \overline{\Psi'_{j,m}\Psi'_{n,i}u'_{m,n}}) - 2\nu\,\overline{u'_{m,i}u'_{m,j}}, \tag{B 1}$$

$$\frac{\bar{\mathrm{D}}F_{ij}}{\bar{\mathrm{D}}t} = F_{ik}G_{kj} + F_{jk}G_{ki} + 2D_{ik}\Omega_{kj} + 2D_{jk}\Omega_{ki} - 2S_{kk}F_{ij} + 2S_{nm}D_{nm}\delta_{ij} - 2S_{nm}L_{inmj} - 2S_{nm}M_{ijnm} - T_{ij}^{\Omega} + (\overline{\Psi'_{i,m}\Psi'_{n,j}u'_{m,n}} + \overline{\Psi'_{j,m}\Psi'_{n,i}u'_{m,n}}) - 2\nu\,\overline{\omega'_{i}\omega'_{j}}. \tag{B 2}$$

Here T_{ij}^{Ω} is the rotational part of the rapid pressure–strain-rate term (see (A 4)) and T_{ij}^{slow} is the slow pressure–strain-rate term,

$$T_{ij}^{\mathrm{slow}} = \frac{2}{\rho}\,\overline{p^{s}s'_{ij}}, \quad p^{s} = -2u'_{m,n}u'_{n,m}, \quad s'_{ij} = \tfrac{1}{2}(u'_{i,j} + u'_{j,i}). \tag{B 3}$$

The fourth-rank tensor $\boldsymbol{L}$ is defined by

$$L_{ijpq} = \int \frac{k_{i}k_{j}k_{p}k_{q}}{k^{4}}E_{nn}(\boldsymbol{k})\,\mathrm{d}^{3}\boldsymbol{k}. \tag{B 4}$$

The triple correlations in (B 1) and (B 2) are trace-free and represent nonlinear intercomponent energy transfer between the D_{ij} and F_{ij}.

The evolution equations of the normalized tensors d_{ij} and f_{ij}, and for the corresponding anisotropies $\tilde{d}_{ij}$ and $\tilde{f}_{ij}$ follow easily from the definitions (3.3) and (3.4) and (B 1) and (B 2). Using the evolution equation for the d_{ij} and that for the normalized Reynolds stress tensor r_{ij}, one can write down the equation for the tensorial difference $\tilde{\Delta}_{ij} = \tilde{r}_{ij} - \tilde{d}_{ij}$. For the case of irrotational mean deformation, this equation is

$$\begin{aligned}\frac{\bar{\mathrm{D}}}{\bar{\mathrm{D}}t}\tilde{\Delta}_{ij} = &-(S_{ik}\tilde{\Delta}_{kj} + S_{jk}\tilde{\Delta}_{ki}) + 2S_{nm}r_{nm}\tilde{\Delta}_{ij} \\ &+2[S_{nm}(M_{imnj} + M_{jmni} + M_{mnij} - L_{mnij}) \\ &+T^{s}_{ij} - \tfrac{1}{2}(\overline{\Psi'_{i,m}\Psi'_{n,j}u'_{m,n}} + \overline{\Psi'_{j,m}\Psi'_{n,i}u'_{m,n}}) - 2\nu(\overline{u'_{i,k}u'_{j,k}} - \overline{u'_{k,i}u'_{k,j}})]/q^2. \end{aligned} \tag{B 5}$$

When the mean strain rate is rapid (inviscid RDT), (B 5) reduces to

$$\frac{\bar{\mathrm{D}}}{\bar{\mathrm{D}}t}\tilde{\Delta}_{ij} = -(S_{ik}\tilde{\Delta}_{kj} + S_{jk}\tilde{\Delta}_{ki}) + 2S_{nm}[r_{nm}\tilde{\Delta}_{ij} + (M_{imnj} + M_{jmni} + M_{mnij} - L_{mnij})/q^2]. \tag{B 6}$$

In addition, one can show that when the velocity spectrum tensor satisfies reflectional symmetry, for example during rapid irrotational deformation of initially isotropic turbulence,

$$M_{imnj} + M_{jmni} + M_{mnij} - L_{mnij} = 0, \tag{B 7}$$

and $\tilde{\Delta}_{ij}$ remains zero when initially so. When the mean strain rate is slow both the nonlinear and viscous terms are in general significant, but special cases exist where the nonlinear effects are relatively weak. For example, in the slowly strained irrotational cases from the simulations of LR the slow pressure–strain term is found to be insignificant relative to the viscous and rapid terms. While information was not reported by LR for the triple correlations in (B 5) there is strong evidence of the insignificance of these terms as well. For example, the insensitivity of the circulicity evolution histories to strain rate, which is particularly strong in the axisymmetric expansion and plane strain cases, suggests that the intercomponent energy transfer between $\tilde{\boldsymbol{d}}$ and $\tilde{\boldsymbol{f}}$ is negligible and of the same level as the slow pressure–strain-rate term. Otherwise, one would expect a stronger dependence of the $\tilde{\boldsymbol{f}}$ histories on the rate of straining in these flows, because the evolution of $\tilde{\boldsymbol{d}}$ is strongly dependent on the rate of strain. The rapid terms in (B 5) involve the fourth-rank tensors $\boldsymbol{M}$ and $\boldsymbol{L}$, but for a simplified analysis these may be modelled with a linear representation in $\tilde{\boldsymbol{d}}$ and $\tilde{\boldsymbol{r}}$ (see Appendix C). KR94 have shown that when these two linear models are used together, the resulting representation of the rapid terms is exact for weakly anisotropic turbulence. In fact for the irrotational flows considered here, this linearized representation of the rapid effects is quite accurate for $C \lesssim 3$. With these simplifying assumptions, we obtain

$$\begin{aligned}\frac{\mathrm{d}\tilde{\Delta}_{ij}}{\mathrm{d}t} = &-\tfrac{5}{7}(S_{ik}\tilde{\Delta}_{kj} + S_{jk}\tilde{\Delta}_{ki}) + \tfrac{10}{21}S_{nm}\tilde{\Delta}_{nm}\delta_{ij} + 2S_{nm}\tilde{r}_{nm}\tilde{\Delta}_{ij} + 2\epsilon_{kk}S^{*}\tilde{\Delta}_{ij} \\ &+2\nu(\overline{u'_{i,k}u'_{j,k}} - \overline{u'_{k,i}u'_{k,j}})]/q^2. \end{aligned} \tag{B 8}$$

The evolution equation for the third-rank tensor Q_{ijk} in inviscid RDT is

$$\begin{aligned}\frac{\bar{\mathrm{D}}}{\bar{\mathrm{D}}t}Q_{ijk} = &-G_{mk}Q_{ijm} - G_{jm}Q_{imk} - \epsilon_{its}G_{sm}M_{jmtk} - \epsilon_{its}G_{mt}M_{jsmk} \\ &+\Omega_z H_{izjk} + 2S_{zm}(Q_{ijkzm} + Q_{izmjk}), \end{aligned} \tag{B 9}$$

where $\Omega_i = \epsilon_{inm}\Omega_{mn}$ is the mean vorticity vector,

$$H_{ijpq} = \overline{\Psi'_{i,p}\Psi'_{j,q}} = \int \frac{k_p k_q}{k^2}\mathscr{F}_{ij}(\boldsymbol{k})\mathrm{d}^3\boldsymbol{k}, \quad H_{ijpp} = F_{ij}, \quad H_{iipq} = D_{pq}, \tag{B 10}$$

and

$$Q_{ijrpq} = \epsilon_{its}\int \frac{k_t k_r k_p k_q}{k^4}E_{sj}(\boldsymbol{k})\,\mathrm{d}^3\boldsymbol{k}, \quad Q_{ijrpp} = Q_{ijr}. \tag{B 11}$$

Details on the definitions (B 10) and (B 11) and the properties of these higher-rank tensors are given in KR94. The stropholysis $\boldsymbol{Q}^*$ can be obtained from $\boldsymbol{Q}$ using (3.8). Alternatively, the RDT transport equation for $\boldsymbol{Q}^*$ can be obtained by a complete symmetrization of (B 9). For the special case of homogeneous turbulence undergoing rapid mean rotation (with no strain), the stropholysis equation is

$$\begin{aligned}\frac{\bar{\mathrm{D}}}{\bar{\mathrm{D}}t}Q^*_{ijk} = {}& \tfrac{1}{18}[\Omega_i(R_{kj}-F_{kj}) + \Omega_j(R_{ki}-F_{ki}) + \Omega_k(R_{ij}-F_{ij})] \\ & + \tfrac{1}{18}[\delta_{kj}\Omega_r(F_{ir}-R_{ir}) + \delta_{ki}\Omega_r(F_{jr}-R_{jr}) + \delta_{ij}\Omega_r(F_{kr}-R_{kr})] \\ & + \Omega_z(M^*_{ijkz}-H^*_{ijkz}) + \tfrac{1}{6}\Omega_z(2\epsilon_{pkz}\,Q^*_{pij} + \epsilon_{pjz}\,Q^*_{pki} - \epsilon_{pki}\,Q^*_{pjz}).\end{aligned} \tag{B 12}$$

Here, $\boldsymbol{M}^*$ is the fourth-rank, fully symmetric, sub-tensor of $\boldsymbol{M}$ defined in (2.3). A relation analogous to (2.3) relates $\boldsymbol{H}$ and its fully symmetric sub-tensor $\boldsymbol{H}^*$. Even in the simple case of rapid mean rotation, the stropholysis equation involves a closure problem, because of the presence of the $\boldsymbol{M}^*$ and $\boldsymbol{H}^*$ terms (see KR94 for a detailed discussion).

Appendix C. Linear structure-based models for weakly anisotropic turbulence

Two simple models that make use of the new tensors are given here because they provide additional insight, but one must keep in mind that more sophisticated structure-based models have been constructed (see KR94 and Reynolds & Kassinos 1995).

A model for the fourth-rank tensor $\boldsymbol{M}$ (see (2.3)) occurring in the rapid pressure–strain-rate term in terms of $\tilde{\boldsymbol{r}}$ alone is fundamentally wrong in non-equilibrium turbulence. For weakly anisotropic turbulence, one can easily construct a model for $\boldsymbol{M}$ that is linear in the anisotropy tensors $\tilde{\boldsymbol{r}}$ and $\tilde{\boldsymbol{d}}$. We first write the most general fourth-rank linear tensor function of two second-rank tensors,

$$\begin{aligned}M_{ijpq}/q^2 = {}& C_1\delta_{ij}\delta_{pq} + C_2(\delta_{ip}\delta_{jq}+\delta_{iq}\delta_{jp}) \\ & + C_3\delta_{ij}\tilde{r}_{pq} + C_4\delta_{pq}\tilde{r}_{ij} + C_5(\delta_{ip}\tilde{r}_{jq}+\delta_{iq}\tilde{r}_{jp}+\delta_{jp}\tilde{r}_{iq}+\delta_{jq}\tilde{r}_{ip}) \\ & + C_6\delta_{ij}\tilde{d}_{pq} + C_7\delta_{pq}\tilde{d}_{ij} + C_8(\delta_{ip}\tilde{d}_{jq}+\delta_{iq}\tilde{d}_{jp}+\delta_{jp}\tilde{d}_{iq}+\delta_{jq}\tilde{d}_{ip}).\end{aligned} \tag{C 1}$$

For homogeneous turbulence, continuity and the definitions fix all of the coefficients in the linear model, and one finds

$$\begin{aligned}M_{ijpq}/q^2 = {}& \tfrac{2}{15}\delta_{ij}\delta_{pq} - \tfrac{1}{30}(\delta_{ip}\delta_{jq}+\delta_{iq}\delta_{jp}) \\ & + \tfrac{4}{21}\delta_{ij}\tilde{r}_{pq} + \tfrac{11}{21}\delta_{pq}\tilde{r}_{ij} - \tfrac{1}{7}(\delta_{ip}\tilde{r}_{jq}+\delta_{iq}\tilde{r}_{jp}+\delta_{jp}\tilde{r}_{iq}+\delta_{jq}\tilde{r}_{ip}) \\ & + \tfrac{11}{21}\delta_{ij}\tilde{d}_{pq} + \tfrac{4}{21}\delta_{pq}\tilde{d}_{ij} - \tfrac{1}{7}(\delta_{ip}\tilde{d}_{jq}+\delta_{iq}\tilde{d}_{jp}+\delta_{jp}\tilde{d}_{iq}+\delta_{jq}\tilde{d}_{ip}).\end{aligned} \tag{C 2}$$

Similar analysis leads to a model for the fourth-rank tensor $\boldsymbol{L}$ (see (B 4)), that is linear in the anisotropy $\tilde{\boldsymbol{d}}$, and with all its numerical coefficients determined by analysis:

$$L_{ijpq}/q^2 = \tfrac{1}{15}(\delta_{ij}\delta_{pq} + \delta_{ip}\delta_{jq} + \delta_{iq}\delta_{jp}) + \tfrac{1}{7}(\delta_{ij}\tilde{d}_{pq} + \delta_{ip}\tilde{d}_{jq} + \delta_{jp}\tilde{d}_{iq} + \delta_{iq}\tilde{d}_{jp} + \delta_{jq}\tilde{d}_{ip} + \delta_{pq}\tilde{d}_{ij}). \quad (C\,3)$$

It is interesting to note that if $\tilde{\boldsymbol{d}} = 0$ then the model above reduces to the linear $\boldsymbol{M}(\tilde{\boldsymbol{r}})$ model with a coefficient $C_5 = -1/7 = -0.143$ in (C 1), *almost exactly the value found by Launder* et al. *(1975) by fitting experimental data*!† A possible explanation is that the anisotropy of the dimensionality in the fitting experiments was much smaller than the anisotropy of the componentality. The results from various direct numerical simulations discussed in earlier sections support this conjecture. This analysis then offers a theoretical basis of the LRR coefficient!

A detailed discussion on the performance of the linear model (C 2) and (C 3) is given in KR94 and Reynolds & Kassinos (1995). For irrotational deformations the model is quite accurate for total strains $C \lesssim 3$, but eventually becomes unrealizable as the basic assumption of weak anisotropy is violated. For rotational flows, stropholysis information must also be included, and KR94 show that the simplest such model is the same as the one given in (C 2) and (C 3), but with the addition of linear stropholysis terms in the representation for $\boldsymbol{M}$,

$$M_{ijpq}/q^2 = \cdots - \tfrac{1}{4}(\epsilon_{ipk}Q^*_{kqj} + \epsilon_{jpk}Q^*_{kqi} + \epsilon_{iqk}Q^*_{kpj} + \epsilon_{jqk}Q^*_{kpi})/q^2. \quad (C\,4)$$

Again all coefficients in the linear model (C 4) are determined by analysis.

REFERENCES

Batchelor, G. K. 1946 The theory of axisymmetric turbulence. *Proc. R. Soc. Lond.* A **186**, 480.

Cambon, C. & Jacquin, L. 1989 Spectral approach to non-isotropic turbulence subjected to rotation. *J. Fluid Mech.* **202**, 295–317.

Cambon, C., Jacquin, L. & Lubrano, J. L. 1992 Toward a new Reynolds stress model for rotation turbulent flows. *Phys. Fluids* A **4**, 812–824.

Chandrasekhar, S. 1950 The theory of axisymmetric turbulence. *Phil. Trans. R. Soc. Lond.* A **242**, 557.

Choi, K.-S. 1983 A study of the return to isotropy of homogeneous turbulence. PhD thesis, Sibley School of Mechanical and Aerospace Engineering, Cornell University, New York.

Craya, A. 1958 Contribution à l'analyse de la trubulence associée à des vitesses moyenees. PhD thesis, Publications Scientifiques et Techniques, Ministère de l'Air France.

Herring, J. R. 1974 Approach of axisymmetric turbulence to isotropy. *Phys. Fluids* **17**, 859–872.

Jeffreys, H. 1931 *Cartesian Tensors*. Cambridge University Press.

Kassinos, S. C. & Reynolds, W. C. 1994 A structure-based model for the rapid distortion of homogeneous turbulence. *Tech. Rep.* TF-61. Thermosciences Division, Department of Mechanical Engineering, Stanford University (referred to herein as KR94).

Kevlahan, N. K.-R. & Hunt, J. C. R. 1997 Nonlinear interactions in turbulence with strong irrotational straining. *J. Fluid Mech.* **337**, 333–364.

Kida, S. & Hunt, J. C. R. 1989 Interaction between different scales of turbulence over short times. *J. Fluid Mech.* **201**, 411–445.

Kim, J., Moin, P. & Moser, B. 1987 Turbulence statistics in fully developed channel flow at low Reynolds number. *J. Fluid Mech.* **3**, 49–58.

Launder, B. E., Reece, G. J. & Rodi, W. 1975 Progress in the development of a Reynolds stress closure. *J. Fluid Mech.* **68**, 537–566 (referred to herein as LRR).

† Note that the tensor a^{mi}_{lj} appearing in Equation (8) in LRR corresponds to $2M_{imlj}$. Then, $\frac{1}{2}\beta = -(2 + 3c_2)/22$ with $c_2 = 0.4$ is the LLR coefficient that corresponds to C_5 in (C 1) above. Thus, the LRR model corresponds to a value of $C_{5_{\mathrm{LRR}}} = -0.145$ in (C 1).

Lee, M. J. & Reynolds, W. C. 1985 Numerical experiments on the structure of homogeneous turbulence. *Tech. Rep.* TF-24. Thermosciences Division, Department of Mechanical Engineering, Stanford University (referred to herein as LR).

Lumley, J. L. & Newman, G. R. 1977 The return to isotropy of homogeneous turbulence. *J. Fluid Mech.* **82**, 161–178.

Mahoney, J. F. 1985 Tensor and isotropic tensor identities. *Matrix Tensor Q*. **34**(5), 85–91.

Moser, R. D., Rogers, M. M. & Ewing, D. W. 1998 Self-similarity of time evolving plane wakes. *J. Fluid Mech.* **367**, 255–289.

Reynolds, O. 1895 On the dynamical theory of incompressible viscous fluids and the determination of the criterion. *Phil. Trans. R. Soc. Lond.* A **186**, 123.

Reynolds, W. C. 1976 Computation of turbulent flows. *Ann. Rev. Fluid Mech.* **8**, 183.

Reynolds, W. C. 1989 Effects of rotation on homogeneous turbulence. In *Proc. 10th Australasian Fluid Mechanics Conference*. University of Melbourne, Melbourne, Australia.

Reynolds, W. C. 1991 Towards a structure-based turbulence model. In *Studies in Turbulence* (ed. T. B. Gatski, S. Sirkar & C. Speziale), pp. 76–80. Springer.

Reynolds, W. C. & Kassinos, S. C. 1995 A one-point model for the evolution of the Reynolds stress and structure tensors in rapidly deformed homogeneous turbulence. *Proc. R. Soc. Lond.* A **451**, 87–104.

Reynolds, W. C. & Kassinos, S. C. 1998 Linear dependencies in fourth-rank turbulence tensor models. *Appl. Math Lett*. **11**(5), 79–83.

Robertson, H. P. 1940 The invariant theory of isotropic turbulence. *Proc. Camb. Phil. Soc.* **36**, 209–223.

Rogers, M. M. & Moin, P. 1987 The structure of the vorticity field in homogeneous turbulent flows. *J. Fluid Mech.* **176**, 33–66.

Rogers, M. M. & Moser, R. D. 1994 Direct simulation of a self-similar turbulent mixing layer. *Phys. Fluids* A **6**, 903–923.

Smith, C. R. & Metzler, S. P. 1983 The characteristics of low-speed streaks in the near-wall region of a turbulent boundary layer. *J. Fluid Mech.* **129**, 27–54.

Tavoularis, S. & Karnik, U. 1989 Further experiments on the evolution of turbulent stresses and scales in uniformly sheared turbulence. *J. Fluid Mech.* **204**, 457–478.

Townsend, A. A. 1976 *The Structure of Turbulent Shear Flow*. Cambridge University Press.